ATMOSPHERIC OPTICAL COMMUNICATIONS IN THE MIDDLE ULTRAVIOLET

by

David Monroe Reilly

SUBMITTED IN PARTIAL FULFILLMENT OF THE REQUIREMENTS FOR THE DEGREE OF MASTER OF SCIENCE

at the

MASSACHUSETTS INSTITUTE OF TECHNOLOGY

May 20, 1976

Signature of Author .....
Department of Electrical Engineering and Computer Science, May 21, 1976

Certified by .....
Thesis Supervisor

Accepted by .....
Chairman, Departmental Committee on Graduate Students

ATMOSPHERIC OPTICAL COMMUNICATIONS IN THE MIDDLE ULTRAVIOLET

by

David Monroe Reilly

Submitted to the Department of Electrical Engineering and Computer Science on May 21, 1976, in partial fulfillment of the requirements for the Degree of Master of Science

ABSTRACT

The performance of atmospheric optical communication systems is, in general, strongly dependent on meteorological conditions. This investigation addresses operation in the middle ultraviolet (2000Å-3000Å) and the use of scattered energy as a means of reducing this dependency.

The atmosphere has been characterized for purposes of optical communications. The basic constituents are gaseous molecules, aerosols and precipitating matter. All possible interactions of optical radiation with the constituents are considered as either coherent scattering or absorption and are completely described by absorption and scattering coefficients and single scatter phase functions. The mid-latitude winter supplement to the standard U.S. Atmosphere was selected as the baseline atmosphere and was augmented by two aerosol models.

A theoretical model to describe the temporal characteristics of scattered radiation, when single scatter conditions prevail, was proposed and developed. The model is based on the focal radii property of a prolate spheroid (the sum of the focal radii is constant for a given surface). It essentially associates all scattering events occurring at a given prolate spheroidal surface with a given instant in time when an impulsive isotropic transmitter is located at one focal point and the receiver at the other. The model was extended to include isotropic, Rayleigh and Mie scattering, where the single scatter phase function for Mie scattering was approximated by the Henyey-Greenstein function. Various combinations of absorption and scattering coefficients, phase function anisotropy, and transmitter/receiver ranges and geometries were evaluated.

Absorption and scattering coefficients and phase functions were computed for the middle ultraviolet based on the selected atmospheric models. It was shown that scattering predominates at 3000Å and absorption at 2000Å and that both scattering and absorption increase as wavelength is decreased. A short wavelength limit on horizontal propagation through the lower atmosphere is established at 2000Å by molecular oxygen absorption. Primary and scattered energy (vs. time) were computed for the model atmospheres when the transmitter and receiver were isotropic and separated by a distance of 0.25 Km. The magnitude of the scattered energy was shown to be almost identical at 2500Å and 3000Å. Primary and primary plus scattered energy were considered as visual range decreased from 23 Km to 5 Km. It was shown that $\simeq$15% change was experienced in primary energy as compared to $\simeq$3% for primary plus scattered if the collection of scattered energy occurred over a one nanosecond interval.

THESIS SUPERVISOR: Cardinal Warde
TITLE: Assistant Professor of Electrical Engineering

Acknowledgments

I would like to thank Professor C. Warde, my thesis advisor, for his guidance throughout this investigation. Also, I would like to extend my gratitude to the individuals whose assistance made this document possible. They are as follows: Professor C. Cooke, for his willingness to discuss various aspects of this investigation and help in clarifying some physical concepts; Warren Clark, for his generous advice and assistance in developing numerical data; and to Karen D'Amore and Debra Norton, for their patience, time and professional preparation of this manuscript. A debt of gratitude is also owed to Raytheon Company (Bedford Laboratories) for their tremendous material support.

TABLE OF CONTENTS

Appendices

Figures and Tables

(by sections)

TABLE OF CONTENTS, continued

TABLE OF CONTENTS, continued

In Section 2, the atmospheric constituents will be identified and associated with appropriate number densities and size distributions. Two specific atmospheric configurations will be selected for use through out this investigation. Section 3 will address the optical properties of the atmosphere i.e. define and describe the possible interactions of electromagnetic energy and the atmospheric constituents. The specific properties for the baseline models will also be determined. The propagation of optical signals thru the atmosphere will be addressed in Section 4. Since it is desired to take advantage of scattered radiation, it becomes imperative to address the temporal response of the atmosphere. A theoretical model for determining the instantaneous intensity of single scattered radiation and the distribution in time of the total collected scattered energy as a function of the optical properties of the atmosphere, transmission and reception geometry and distance between transmitter and receiver is proposed, developed and applied for the baseline atmospheric model in the middle ultraviolet region. Section 5 briefly addresses the operational background and Section 6 contains conclusions and recommendations.

SECTION 2 - ATMOSPHERIC CONSTITUENTS

---

1. INTRODUCTION

The atmosphere may be thought of as molecular gas in which solids and liquids are suspended (aerosols) and from/through which liquids and solids may be percipitating. The exact make-up of the atmosphere at a given point and time is a function of geographical location, altitude, time of day and time of year, weather (humidity, wind, temperature, etc.) and the degree and type of human activity (farming, urban, industrial, etc.) in the general area. This section will be mainly concerned with the physical properties of the atmosphere. Optical properties will be covered in Section 3.

2. GASEOUS MOLECULES

The important molecular species (for purposes of ultraviolet communications) are: nitrogen, oxygen, carbon dioxide, nitrous oxide, methane, carbon monoxide, water vapor and ozone. The number densities of these molecules are relatively stable, except for water vapor and ozone.

The sea level configuration of the "Mid-Latitude Winter Supplement"[1] to the U.S. Standard Atmosphere, 1962, was selected as the baseline atmospheric model for this investigation. The

molecular species and their number densities are listed in Table 1. Pertinent physical characteristics are listed in Table 2.

3. SUSPENDED PARTICLES (AEROSOLS)

The Suspended Particles are a result of natural processes and human activity.[3][4] They include hydroscopic, dust-like and organic substances as well as water droplets and ice crystals, and range in size (radius) between $10^{-3}\mu m$ and $10^{2}\mu m$. Variations in the number density, size distribution and complex index of refraction of these particles are responsible for the large variations in the optical properties of the atmosphere. Numerous groups are presently attempting to establish the origin, production and annihilation rates, properties and the functional dependencies of these particles on meteorological conditions, human activity, etc.

For purposes of analytically determining the propagation characteristics of optical radiation through the atmosphere, several properties of the aerosol must be available, most important of which are particle size distribution, number density, shape and complex index of refraction. A recent paper by E. Shettle and R. Fenn[5] summarizes the present understanding of the subject and proposes three general model (rural, urban and maritime) which are based on considerable experimental evidence. The size distributions for these models are expressed by mathematical functions and remain constant for visual ranges between 2 Kms and 50 Kms. The number densities are proportional to visual range.

Molecule	Chemical Formula	Number Density cm^{-3}	(cm-atm) stp/Km Horizontal path @S.L.
Nitrogen	N_2	2.10×10^{19}	7.808×10^{4}
Oxygen	O_2	5.63×10^{18}	2.095×10^{4}
Carbon Dioxide	CO_2	8.87×10^{15}	33
Nitrous Oxide	N_2O	7.28×10^{12}	0.028
Methane	CH_4	4.30×10^{13}	0.16
Carbon Monoxide	CO	2.03×10^{12}	0.0075
Water Vapor	H_2O	1.17×10^{17}	
Ozone	O_2	6.7×10^{11} (2)	
Air	---	2.69×10^{19}	10^{5}

Table 1 - Molecular Density Data for the Mid-Latitude Winter Supplement to the U.S. Standard Atmosphere at Sea Level

Geometric Altitude:	0.0 m
Temperature:	272.2°K
Pressure:	1.018×10^{3} mb
Density:	1.301 Kg m^{-3}
Molecular Weight:	28.97
Particle Speed:	458.9 m sec^{-1}
Collision Frequency:	6.92×10^{9} sec^{-1}
Mean Free Path:	6.63×10^{-8} m

Table 2 - Pertinent Physical Characteristics for the Mid-Latitude Winter Supplement to the U.S. Standard Atmosphere at Sea Level

Since a large percentage of the particles are hydroscopic (60-70%), it is expected that the size distribution will vary as a function of the amount of water vapor present in the atmosphere. Several investigations[6][7] claim that the shift in size distribution is negligible below a relative humidity value of 0.7 and that the size of the hydroscopic particles may increase by as much as a factor of 10 between relative humidity values of 0.7 and 1.0. A rough estimate of visual range based on relative humidity indicates that visual range will be less than 1-2 Kms when relative humidity is greater than 0.7. When the visual range is less than 1-2 Kms, the description of the number densities and size distributions of both the suspended and precipitating particles become quite complex and hasn't to the author's knowledge been analytically described.

For purposes of this investigation, the molecular gas model defined in Part 1 will be augmented by two aerosol models[2] which closely correspond to the "rural" model discussed above. Visual ranges of 5 Kms ("hazy") and 23 Kms ("clear") corresponding to 1.378×10^4 and 2.828×10^3 particles cm^{-3} will be utilized. The size distribution is the same for both the 5 Km and 23 Km models and is shown in Figure 1. The density function $n(r)/\Delta r$ has been normalized to 1 particle per cm^3.

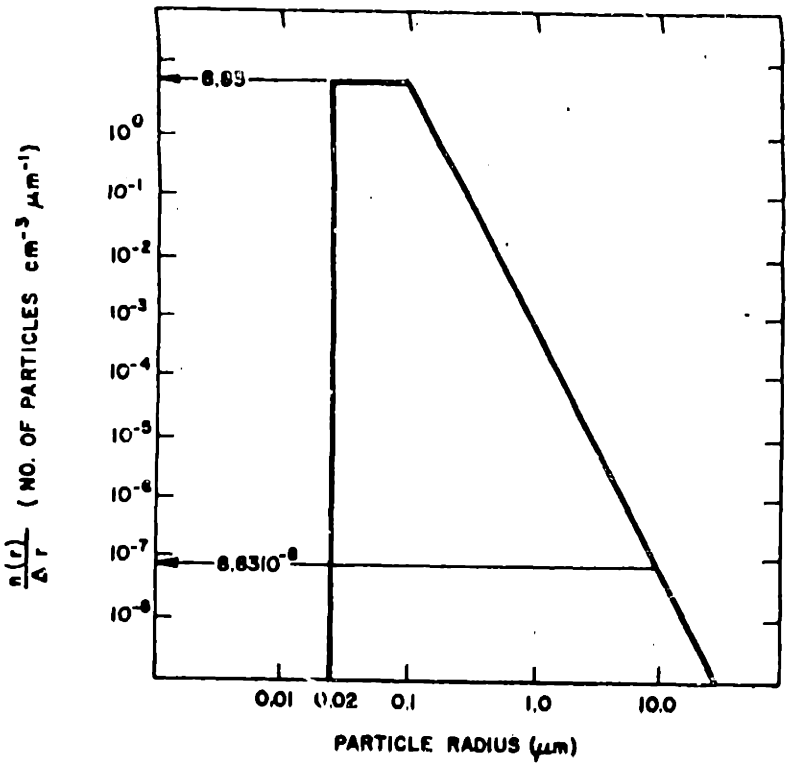

Figure 1. Aerosol Size Distribution Used in Computing Attenuation Coefficients

From: Atmospheric Attenuation of Laser Radiation From 0.76 to 31.25μm; Figure 1
R. McClatchey & J. Selby
3 January 1974; AFCRL-TR-74-0003

$$\frac{n(r)}{\Delta r} = \begin{cases} C_1 10^4; & 0.02\mu m \leq r \leq 0.1\mu m \\ C_1 r^{-4}; & 0.1\mu m \leq r \leq 100\mu m \\ 0; & r<0.02\mu m \ \& \ r>100\mu m \end{cases}$$

(Particles μm^{-1})

$$C_1 = 8.83 \times 10^{-3}$$

Figure 1 - Aerosol Size Distribution

References

1. S.L. Valley - Scientific Editor, Handbook of Geophysics and Space Environments, 1965, McGraw-Hill.

2. R.A. McClatchey and J.E.A. Selby, Atmospheric Attenuation of Laser Radiation from 0.76 to 31.25μm, 3 January 1974, AFCRL-TR-74-0003.

3. G.V. Rosenberg, "Optical Investigation of Atmospheric Aerosol," Soviet Physics Uspekhi, Vol. 11, No. 3, Nov-Dec, 1968.

4. K. Bullrich, "Scattered Radiation in the Atmosphere and the Natural Aerosol," Advances in Geophysics, Vol. 10, Edited by H. Landsberg and J. Van Mieghem, 1964, Academic Press.

5. E.P. Shettle and R.W. Fenn, Models of the Atmospheric Aerosols and Their Optical Properties, AGARD's Technical Meeting on "Optical Propagation in the Atmosphere," 27-31, October 1975, Lyngby, Denmark.

6. F.E. Volz, "Infrared Refractive Index of Atmospheric Aerosol Substances," Applied Optics, April 1972, Vol. 11, No. 4.

7. E.A. Barnhardt and J.L. Streete, "A Method for Predicting Atmospheric Aerosol Scattering Coefficients in the Infrared," Applied Optics, June 1970, Vol. 9, No. 6.

SECTION 3 - OPTICAL PROPERTIES

---

1. INTRODUCTION

The interaction of optical radiation with the atmospheric constituents (gaseous molecules and suspended and precipitating matter) modifies the primary radiation field (that portion of the transmitted field which has not underwent an interaction with

the constituents). The variations in the magnitude of these interactions due to varying meteorological conditions are dramatic. Rosenberg[1] states that "the scattering coefficient of air in the visible region of the spectrum changes approximately from 10^{-2} km^{-1} for barely noticeable haze to 10^{4} km^{-1} for extreme dense fogs, i.e. by a factor of 10^{6}." The primary cause for these changes is variations in the number densities, size distributions and the complex index of refraction of the suspended particles.

For purposes of this investigation all interactions are classified as either coherent scattering or absorption. In the case of coherent scattering, energy lost to the primary field is gained by a scatter field which is at the same wavelength as the primary field. Absorption includes all other interactions (true absorption, incoherent scattering, dissociation, etc.) where the "absorbed" energy is essentially lost to the useful radiation field (primary plus coherently scattered radiation).

In this section, expression will be developed for the interaction coefficients (absorption, scattering and extinction) which describe the magnitude of the interactions and for the single scatter phase functions which describe the spatial distribution of scattered energy. Specific values for the coefficients will be generated for the middle ultraviolet spectral region where the atmosphere will be characterized by the mid-latitude winter supplement to the U.S. Standard atmosphere augmented by the two AFCRL aerosol models which were described in Section 2.

The sum of the scattering and absorption coefficients is called the extinction (volume) or total attenuation coefficient since it determines the magnitude of the primary field loss. It may be thought of as the effective blocking area per unit volume. An appreciation for the above coefficients may be obtained by considering the Bouger-Lambert Law[2] which states that the fractional decrease in the intensity of a collimated beam due to its passage thru matter is proportional to distance. The constant of proportionality is the extinction coefficient; i.e.

$$\frac{dI}{I} = -kdl = -(k_A + k_s)dl$$

where: k (cm^{-1}) is the extinction coefficient.

In general the coefficients and single scatter phase functions are obtained thru combined analytical and experimental techniques. For gaseous molecules where the radius of the particles (typically 2-5Å) is much less than the wavelength of optical radiation the scattering coefficient and phase function are obtain from Rayleigh's fourth power scattering law. The absorption cross-sections are experimentally determined for the various molecules present and then in conjunction with their respective number densities they are summed to obtain the absorption coefficient for the gas. For aerosols where the radius of the particles is on the order of (or greater than) the wavelenth of the optical radiation, experimental

data on the number densities, size distribution and complex index of refraction are required before the coefficients and the single scatter phase function may be calculated via Mie's Theory[3]. The coefficients and phase functions are functions of wavelength, particle size distribution, number density and complex index of refraction. The coefficients which characterize a given medium are the sum of those associated with each type of constituent; e.t.

$$K = K_A + K_s \qquad (cm^{-1})$$

$$= K_{A_m} + K_{A_a} + K_{s_m} + K_{s_a} \qquad cm^{-1}$$

where:

- the subscripts refer to:
  - A: Absorption
  - S: Scattering
  - a: aerosol
  - m: molecular
- K = extinction coefficient
- K_A = absorption coefficient
- K_s = scattering coefficient

The coefficients and phase functions are now developed for the middle ultra-violet spectral region based on the atmospheric models described above.

2. GASEOUS MOLECULES

(a) Molecular Scattering

Molecular scattering is described by Rayleigh's fourth-power law of scattering. This law is a limiting case of the more

general solution by Mie where $r \ll \lambda$ i.e. the radius of the particles (typically 2-5Å for gaseous molecules) is much less than the wavelengh of the incident radiation. The scattering coefficient is defined[4] as:

$$K_S = \frac{8\pi^3}{3N} \frac{(n^2-1)^2}{\lambda^4} \left(\frac{6 + 3\rho_n}{6 - 7\rho_n}\right) \quad cm^{-1}$$

where: n = index of refraction

N number density of the molecules

ρ_n = depolarization factor

$\left(\frac{6 + 3\rho_n}{6 - 7\rho_n}\right)$ = depolarization term which expresses the influence of the optically anisotropic molecules on scattering.

Goody[5] has calculated the scattering cross-sections and coefficients (@0°C and 1013 mb) based upon Penndorf's tables[4]. These values are listed in table 1 for the wavelengths of interest.

As a result of scattering interactions with particle(s) a scatter radiation field is established about the particle(s). In general it is not distributed symmetrically in space and is described by a single scatter (scalar) phase function $p(\cos \theta_s)$ where θ_s is the scattering angle (determined by the forward direction of the incident waves, the scattering point and the direction of observation). The phase function is normalized such

Wavelength λ (Å)	Scattering Cross-Section σ_s (cm^2)	Scattering* Coefficients K_s (cm^{-1})
2000	3.551×10^{-25}	9.542×10^{-6}
2100		
2200		
2300		
2400		
2500	1.258×10^{-25}	3.382×10^{-6}
2600		
2700		
2800		
2900		
3000	5.676×10^{-26}	1.525×10^{-6}

* The scattering coefficient is based on 2.69×10^{19} molecules/cm^3.

TABLE 1: Molecular Scattering Cross-Sections and Coefficients

that:

$$\frac{K_S}{4\pi} \int_{\Omega} p(\cos\theta_s)\, d\Omega = K_S \quad (cm^{-1})$$

The scalar phase function (Rayleigh phase function) which describes the spatial distribution of radiation scattered from gaseous molecules is:

$$p(\cos\theta_s) = \frac{3}{4}(1 + \cos^2\theta_s)$$

Figure 1 is a plot of this function versus θ_s.

(b) Molecular Absorption

In the 2000Å - 3000Å spectral region electromagnetic fileds interact with the electronic structure (versus vibrational or rotational structure) of the atmospheric molecules. Of the eight molecules noted in Section 2 (N_2, O_2, CO_2, N_2O, CH_4, CO, H_2O and O_3), absorption only need be considered for Ozone (O_3) and molecular oxygen (O_2).

Absorption by a single molecule is characterized by its absorption cross-section (σ_A). "Total absorption" cross-section (σ_T) data (total absorption is identical to extinction) is obtained experimentally and then adjusted by substracting out the coherent scatter (Rayleigh scatter) contribution σ_S to obtain σ_A ($\sigma_A = \sigma_T - \sigma_S$).

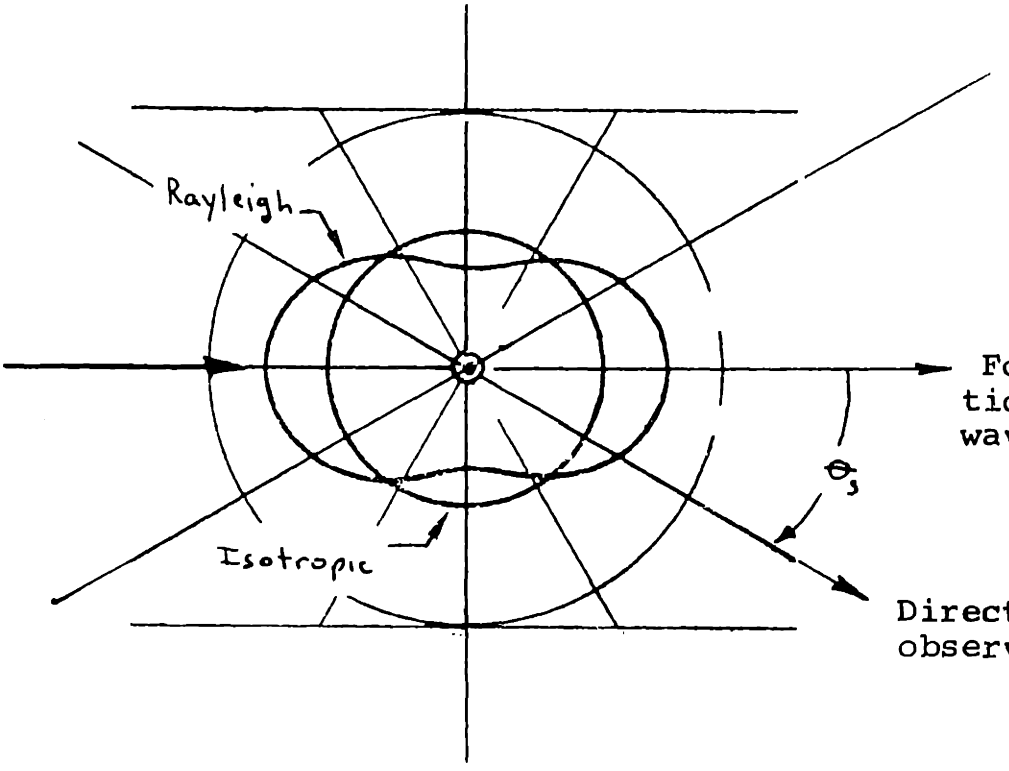

Rayleigh: $p(\cos\theta_s) = 3/4\ (1+\cos^2\theta_s)$

Isotropic: $p(\cos\theta_s) = 1$

where: θ_s = scattering angle

FIGURE 1: Single Scatter (Scalar) Phase Functions for Molecular and Isotropic Scattering (Phase diagram)

The absorption coefficient for a given gas mixture is obtained by multiplying the appropriate cross-section with it's respective number density and then summing the contribution from each specie; i.e.

$$K_A \text{ (molecular)} = \sum_{i=1}^{n} \kappa_i N_i \qquad \text{cm}^{-1}$$

$$K_A \text{ (molecular)} = \sigma_A(O_2)N_{O_2} + \sigma_A(O_3)N_{O_3} \qquad \text{cm}^{-1}$$

where: $N_{O_2} = 5.63 \times 10^{18}$ molecules/cm^3

$N_{O_3} = 6.70 \times 10^{11}$ molecules/cm^3.

Absorption by ozone (O_3) consists of a strong continuum component with weak bands (Hartley bands) superimposed[6]. In the 2000Å - 3000Å region greatest absorption occurs at λ = 2553 Å where $_T = 1.16 \times 10^{-17}$ cm^2. Figure 2 is a plot of total absorption cross-section (σ_T) verses wavelength. Due to the relative magnitude of the coherent scatter contribution ($\sigma_s = 3.551 \times 10^{-25}$ cm^2 @ 2000Å and 5.676×10^{-26} cm^2 @ 3000Å) to the total absorption cross-section, the scatter contribution may be neglected and σ_T will be approximately equal to σ_A. Values for the absorption cross-section and coefficient are listed in Table 2.

Absorption by molecular oxygen is negligible for 2600Å $\leq \lambda \leq$ 3000Å; however, below 2600Å the weak Herzberg dissociation continuum[6] sets in and gradually increases the total absorption cross-section as wavelength decreases. Although the

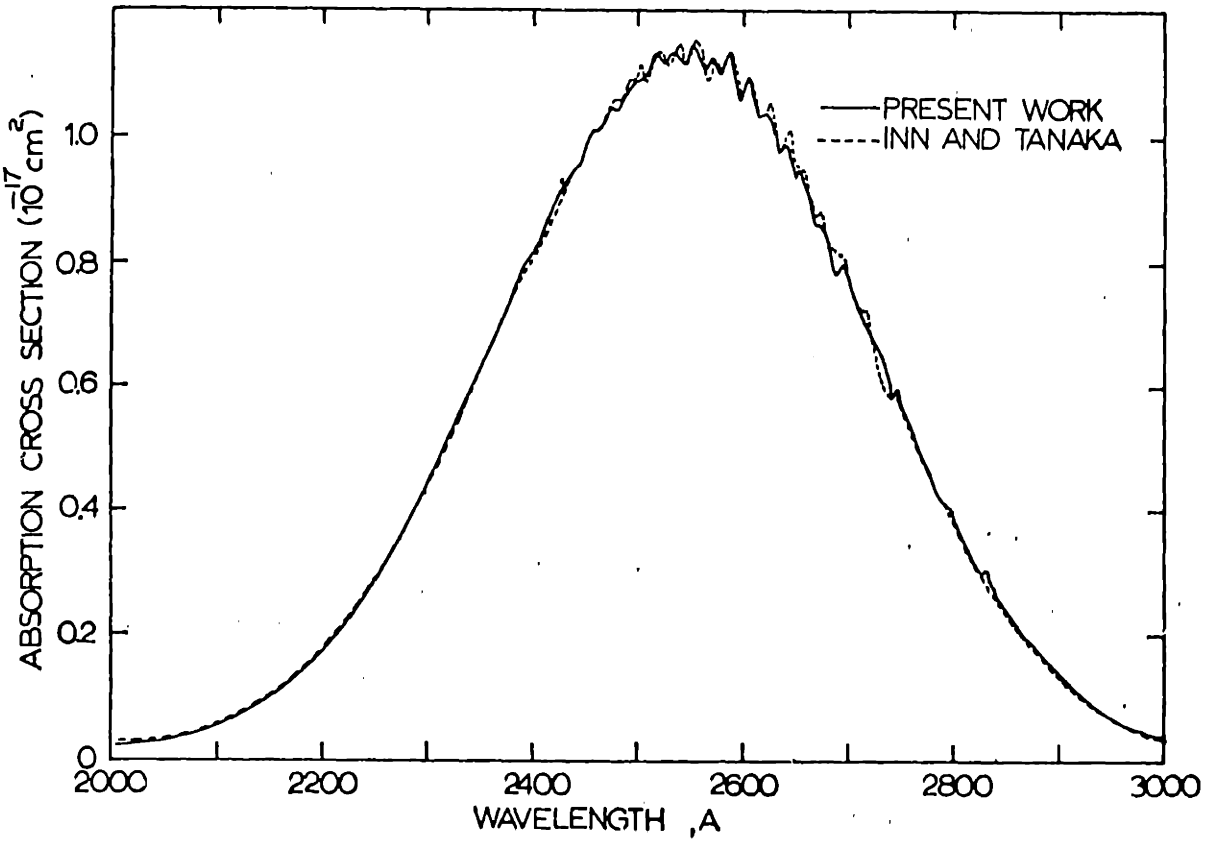

Fig. 44. Comparison of measured total absorption cross section data for O_3 between 2000 and 3000 A (from *Griggs* [1968]); solid line, *Griggs* [1968]; dashed line, *Inn and Tanaka* [1953].

FROM: Critical review of Ultraviolet photoabsorption cross-sections for Molecules of Astrophysical and Aeronomic Interest; R.D. Hudson; NSRDS - NBS 38; Issued August 1971; Figure 44, P-69.

FIGURE 2: Ozone, Total Absorption Cross-Section

Wavelengh λ (Å)	Absorption Cross-Section σ_A (cm^2)	Absorption Coefficient* K_A (cm^{-1})
2000	3.20×10^{-19}	2.14×10^{-7}
2100	5.47×10^{-19}	3.67×10^{-7}
2200	1.80×10^{-18}	1.21×10^{-6}
2300	4.54×10^{-18}	3.04×10^{-6}
2400	8.03×10^{-18}	5.38×10^{-6}
2500	1.11×10^{-17}	7.44×10^{-6}
2553	1.16×10^{-17}	7.77×10^{-6}
2600	1.10×10^{-17}	7.37×10^{-6}
2700	7.62×10^{-18}	5.11×10^{-6}
2800	3.72×10^{-18}	2.49×10^{-6}
2900	1.33×10^{-18}	8.91×10^{-7}
3000	3.59×10^{-19}	2.41×10^{-7}

* The absorption coefficient is based on 6.70×10^{11} molecules/cm^3

TABLE 2: Absorption Cross-Sections and Coefficients for Ozone

total absorption cross-section for O_2 is much smaller than that at O_3, the number density of O_2 causes a large absorption coefficient. Figure 3 is a plot of total absorption cross-section verses wavelength. For oxygen, the contribution of the coherent scatter cross-section (σ_s) to the total absorption cross-section (σ_T) may not be neglected and therefore, must be substracted out to obtain the absorption cross-section (σ_A). Values for σ_T, σ_A and the absorption coefficients K_A are listed in Table 3.

(c) Interaction Coefficients

The interaction coefficients for the molecular gas defined by the mid-latitude winter supplement to the standard U.S. Atmosphere are listed in Table 4. The coefficients are related as follows:

$$K_A = K_A(O_2) + K_A(O_3) \qquad cm^{-1}$$

$$K = K_A + K_S \qquad cm^{-1}$$

3. AEROSOLS

The aerosols represents a polydispersed suspension or, a suspension of varying size absorbing/scattering particles. For purposes of this investigation the particles will be considered as homogeneous spheres posessing a complex index of refraction where the particle size distribution is described by an appropriate function. To characterize their interaction with electromagnetic

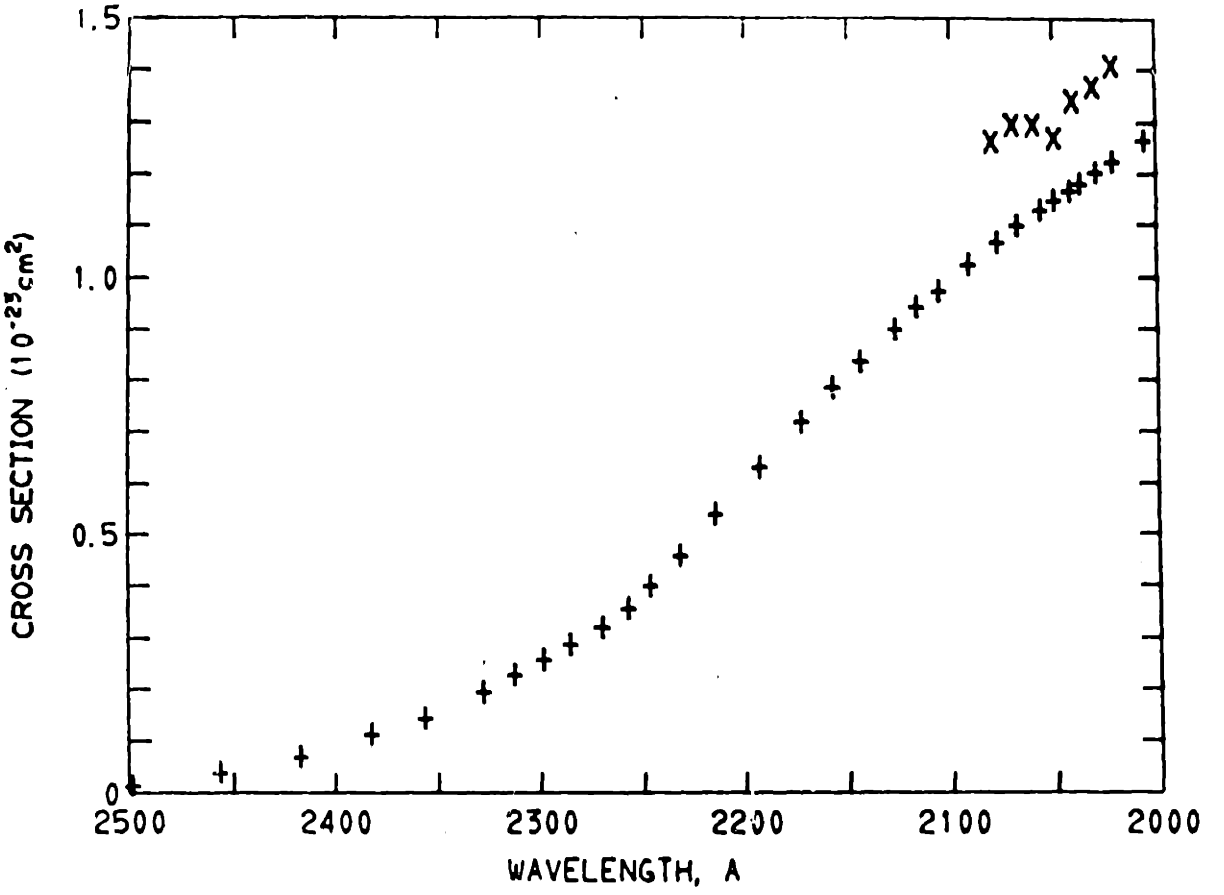

Fig. 11. Comparison of measured total absorption cross sections for O_2 between 2000 and 2500 A; +, *Ditchburn and Young* [1962]; ×, *Blake et al.* [1966].

FROM: Critical review of Ultraviolet Photoabsorption Cross-Sections for Molecules of Astrophysical and Aeronomic Interest; R.D. Hudson; NSRDS - NBS 38; Issued August 1971; Figure 11, P. 32.

FIGURE 3: Oxygen, Total Absorption Cross-Section

Wavelength λ(A)	Total Absorption Cross-Section σ_T (cm^2)	Absorption Cross-Section σ_A (cm^2)	Absorption* Coefficient K_A (cm^{-1})
2000	1.3×10^{-23}	1.27×10^{-23}	7.15×10^{-5}
2100	1.0×10^{-23}		
2200	6.0×10^{-24}		
2300	2.5×10^{-24}		
2400	9.0×10^{-25}		
2500	2.0×10^{-25}	7.42×10^{-26}	4.21×10^{-7}

* The absorption coefficient is based on 5.63×10^{18} O^2 molecules/cm^3

TABLE 3: Absorption Cross-Sections and Coefficients for Molecular Oxygen

Wavelength λ(Å)	Scattering Coefficient K_S (cm^{-1})	Absorption Coefficient K_A (cm^{-1})	Extinction Coefficient K (cm^{-1})
2000	9.542×10^{-6}	7.17×10^{-5}	8.12×10^{-5}
2100			
2200			
2300			
2400			
2500	3.382×10^{-6}	7.86×10^{-6}	1.12×10^{-5}
2600			
2700			
2800			
2900			
3000	1.525×10^{-6}	2.41×10^{-7}	1.76×10^{-6}

TABLE 4: Interaction Coefficients for the Molecular Gas Defined by the Mid-Latitude Winter Supplement to the Standard U.S. Atmosphere

radiation requires that the scattering and absorption coefficients and the single phase scattering function be known. Due to the range of the particle sizes being considered ($.02\mu m \leq r \leq 100\mu m$) and the wavelengths of interest ($0.2\mu m \leq \lambda \leq 0.3\mu m$) the asymptotic approaches (i.e. Rayleigh fourth power law when $r << \lambda$ or geometric optics when $r >> \lambda$) do not apply and a rigerous solution of Maxwell's equations is required. Since the particles are being considered as spherical and homogeneous, the solutions of Mie[3] maybe utilized to derive the cross-section and the phase function for a single particle of a given size parameter ($x=2\pi r/\lambda$) and complex index of refraction. Since interference between particles may be neglected (center-to-center distances of separation greater than 3 radii)[2] the absorption and scattering coefficients and the phase function for the polydispersed suspension are the sums of the individual particle contributions in a unit volume.

The steps and equations involved are discussed in subsequent paragraphs. The approach is similar to that of Hottel and Sarofim[2], Van De Hulst[3] and Deirmendjian[7]. Actual values will not be calculated.

(a) Scattering From A Homogeneous Spherical Particle

When electromagnetic radiation impinges on a homogeneous spherical partical possessing a complex index of refraction, some of that radiation will be absorbed and some will be scattered. The absorption (σ_A) and scattering (σ_s) cross-sections and the scattering phase function [$p(\theta)$] characterize these interactions with the particle and are derived as follows:[2]

Let the radiation scattered from the particle be:

$$p(\theta_s)\ \frac{\sigma_s}{4\pi}\ I = \frac{1/2}{(2\pi/\lambda)^2}\ \left[i_\perp(\theta_s) + i_{11}(\theta_s) \right] I \quad \frac{\text{watt}}{\text{sr}}$$

$$\longrightarrow p(\theta_s) = \frac{\lambda^2}{2\pi\sigma_s}\ \left[i_\perp(\theta_s) + i_{11}(\theta_s) \right]$$

where:
- θ_s is the scattering angle
- I is the intensity incident on the particle
- $i_\perp(\theta_s)$ and $i_{11}(\theta_s)$ are dimensionless intensities corresponding to component perpendicular and parallel to the scattering plane respectively.

The dimensionless intensities $i_\perp(\theta_s)$ and $i_{11}(\theta_s)$ are functions of the size parameter ($x = 2\pi r/\lambda$), the complex index of refraction (n') and the scattering angle (θ_s). They are represented by infinite series as shown below:

$$i_\perp(\theta_s) = \left[\sum_{m=1}^{\infty} \frac{2m+1}{m(m+1)} \left(A_m \pi_m + b_m \tau_m \right) \right]^2$$

$$i_{11}(\theta_s) = \left[\sum_{m=1}^{\infty} \frac{2m+1}{m(m+1)} \left(A_m \tau_m + b_m \pi_m \right) \right]^2$$

where: A_m and b_m are the amplitude functions and π_m and τ_m are the angular functions.

The extinction, scattering and absorption cross-sections are defined in terms of the amplitude and angular functions as follows:

$$2\pi r\,\sigma = \frac{2}{x^2} \sum_{m=1}^{\infty} (2m+1)\ \mathrm{Re}\ (A_m + b_m)$$

$$2\pi r\,\sigma_s = \frac{2}{x^2} \sum_{m=1}^{\infty} (2m+1) \left(|A_m|^2 + |b_m|^2 \right)$$

$$\sigma_A = \sigma - \sigma_s$$

The derivation of the amplitude and angular functions is briefly discussed below to give an appreciation of the magnitude of the task. Dave[8] has prepared a computer program which generates the interaction coefficients and phase function via Mie's theory.

(1) Angular functions π_m and τ_m:

These functions are derived from the legendre polynominals.

$$\pi_m (\cos\theta_s) = \frac{d}{d(\cos\theta_s)} P_m (\cos\theta_s)$$

$$\tau_m (\cos\theta_s) = \cos\theta_s\, \pi_m (\cos\theta_s) - \sin^2\theta \frac{d}{d\cos\theta_s} \pi_m(\cos\theta_s)$$

P_m, the legendre polynominals, are a finite series defined by:

$$P_m(x) = \frac{1}{2^m\, m}\ \frac{d^m (x^2-1)^m}{d x^m}$$

(2) Amplitude functions A_m and b_m:

$$A_m = \frac{S_m'(y)\, S_m(x) - n'\, S_m'\, S_m'(x)\, S_m(y)}{S_m'(y)\, \phi_m(x) - n'\, \phi_m'(x)\, S_m(y)}$$

$$b_m = \frac{n'\, S_m'(y)\, S_m(x) - S_m'(x)\, S_m(y)}{n'\, S_m'(y)\, \phi_m(x) - \phi_m'(x)\, S_m(y)}$$

where:

- $y = n'\, x$
- $x = \frac{2\pi r}{\lambda}$
- $S_m(Z) = \left(\frac{\pi Z}{2}\right)^{1/2} J_{m+1/2}(Z)$
- $C_m(Z) = (-1)^m\ (\pi Z/2)^{1/2}\ J_{-m-1/2}(Z)$
- $J_{m+1/2}$ and $J_{-m-1/2}$ are Bessel functions of the positive and negative half orders.
- $\phi_m(Z) = S_m(Z) + i\, C_m(Z)$
- $S_m'(Z) = \frac{\partial}{\partial Z}\ S_m(Z)$
- $\phi_m'(Z) = \frac{\partial}{\partial Z}\ \phi_m(Z)$

(b) Scattering From a Polydispersed Suspension

The size distribution of the suspended particles is described by a function n(r) where n(r)dr is the number of particles per unit volume having a characteristic dimension between r and r+dr. Since interference between particles may be neglected (center-to-center distance of separation greater than 3 radii)[2], the absorption and scattering coefficients and the phase function for the polydispersed suspension are the sums of the individual particle contribution in a unit volume as shown below:

$$K_A = \int_{r_1}^{r_2} n(r)\ \sigma_A(r)\ dr \qquad cm^{-1}$$

$$K_S = \int_{r_1}^{r_2} n(r)\ \sigma_S(r)\ dr \qquad cm^{-1}$$

$$p(\theta) = \frac{1}{K_S} \int_{r_1}^{r_2} n(r)\ \sigma_S(r)\ p(\theta, r)\, dr$$

where: r_2 and r_1 are the upper and lower limits on the particle size distribution.

$\sigma_A(r)$, $\sigma_S(r)$ and $p(\theta, r)$ are the cross-sections and phase function for a single particle of radius r.

In reality $\sigma_A(r)$, $\sigma_S(r)$ and $p(\theta, r)$ are computed for a number of values of r and the integration is accomplished

numerically. It is important that the size of the intervals between discrete values of r be sufficiently small in order to obtain the correct results. This subject has been discussed in some detail by Dave [9] [10].

(c) Representation of the Aerosol SingleScatter Phase Function by the Henyey-Greenstein Function.

For radiative transfer calculations, a simple analytical expression for the scalar phase function is desirable. The Henyey-Greenstein function is such a function.[11][12] This function is defined as follows:

$$P(\cos\theta_S) = \frac{1 - g^2}{(1 + g^2 - 2g\cos\theta_S)^{3/2}}$$

where: g is the average value of the cosine of the scattering angle θ_S ($g = \overline{\cos\theta_S}$).

An anisotropy parameter γ has been defined by La Rocca[11] which equals the fraction of the radiation scattered into a forward hemisphere. γ is defined as follows:

$$\gamma = \frac{1}{4\pi} \int_0^{2\pi} \int_0^{1} \frac{1 - g^2}{(1 + g^2 - 2g\cos\theta_S)^{3/2}} d(\cos\theta_S)\, d\phi$$

The function is plotted versus the scattering angle in Figure 4. A comparison between an actual phase function computed via Mie

FROM: Atmospheric Transmittance and Radiance: Methods of Calculation: A. LaRocca and R. Turner; ERIM, June 1975

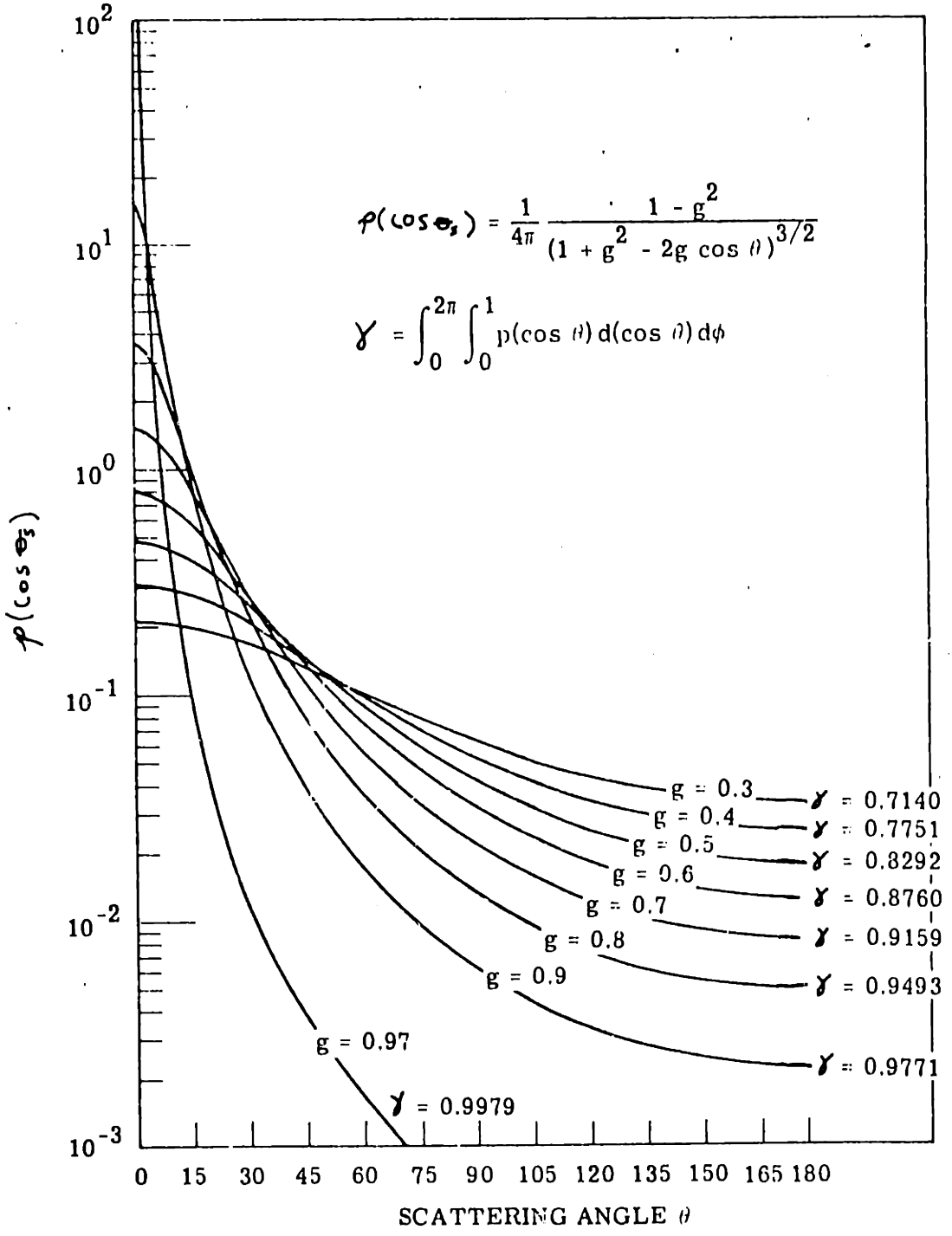

HENYEY-GREENSTEIN PHASE FUNCTION FOR DIFFERENT VALUES OF THE ANISOTROPY PARAMETER γ

FIGURE 4: Henyey-Greenstein Phase Function Versus the Scattering Angle Θ_s

theory by Deirmendjian[7] and the Henyey-Greenstein representation is shown in Figure 5. It is also noted that this function reduces to the isotropic phase function [$P(\cos\Theta_s) = 1$] when $g = 0$.

Since there is a close connection between the energy loss due to scattering and absorption and the amplitude of the scattered radiation in the forward direction[13], one should be able to select the proper valve of "g" for the Henyey-Greenstein function based on knowledge of the extinction coefficient which characterizes the medium. The basic relation's are contained in Van De Hulst's extinction theorem[3][7] and the cross-section theorem of quantum mechanics.

(d) Interaction Coefficients for the AFCRL Aerosol Models

The number density and size distribution of the two AFCRL Aerosol models (5 Km and 23 km visual range) were noted in Section 2. The complex index of refraction[14] and the interaction coefficients for λ = 2000Å, 2500Å and 3000Å are listed in Table 5.

4. COMPOSITE MOLECULAR AND AEROSOL MODEL

The Mid-Latitude winter supplement to the U.S. standard atmosphere and the two AFCRL aerosol models have been combined in order to generate two realistic atmospheric models. The interaction coefficients at λ = 2000Å, 2500Å and 3000Å for the

FROM: Atmospheric Transmittance and Radiance: Methods of Calculation; A. La Rocca and R. Turner; ERIM, June 1975

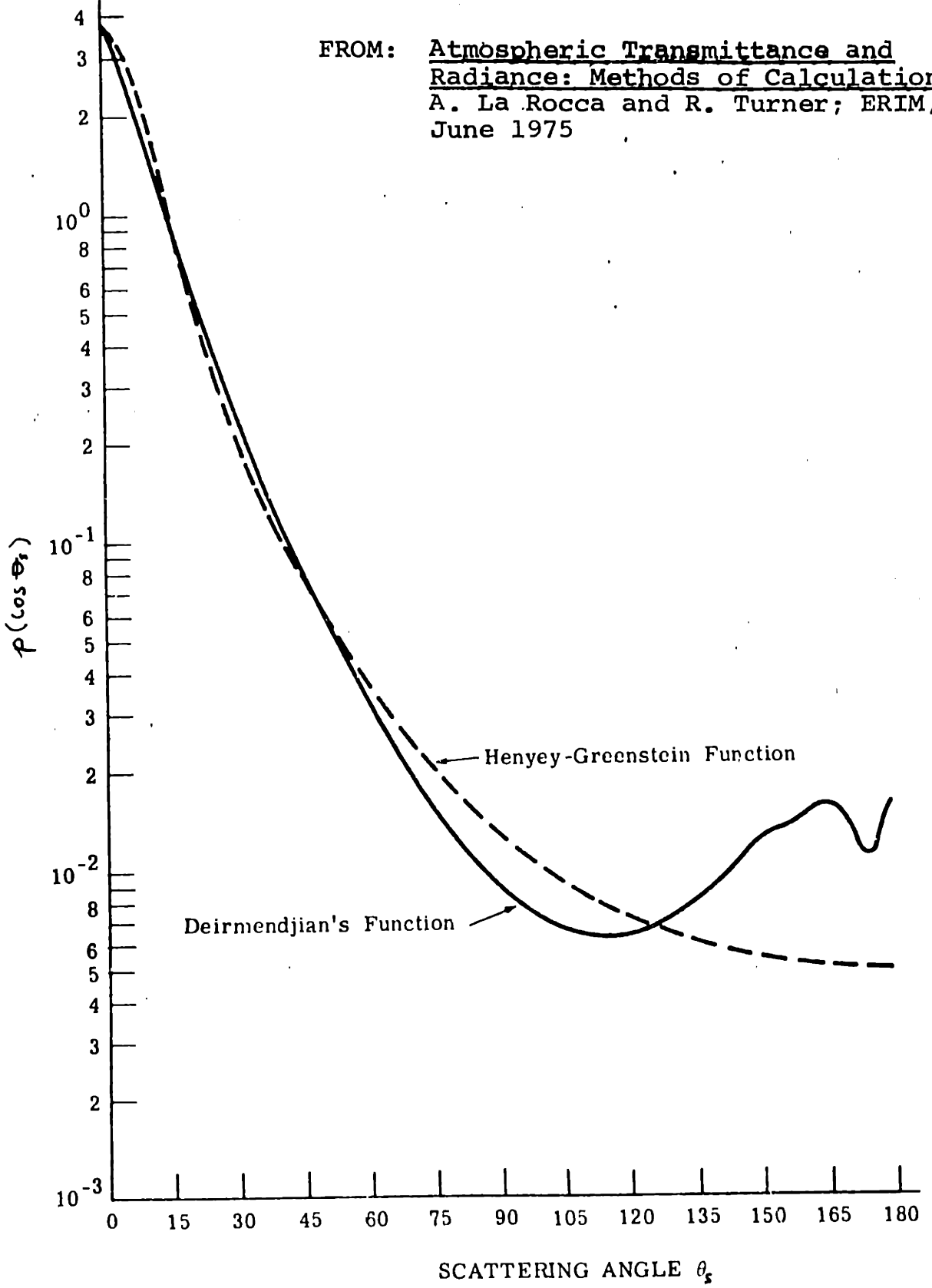

COMPARISON OF DEIRMENDJIAN'S PHASE FUNCTION FOR WATER HAZE L AT $\lambda = 0.45\ \mu m$ AND THE HENYEY-GREENSTEIN PHASE FUNCTION WITH ANISOTROPY PARAMETER $\gamma = 0.9493$

FIGURE 5: Comparison of Henyey-Greenstein Function With Phase Function Computed via Mie Theory

Wavelength λ (Å)	Index of Refraction Real	Imaginary	Visual Range (km)	Scattering Coefficient K_S (cm^{-1})	Absorption Coefficient K_A (cm^{-1})	Extincti Coeffici K (cm^{-}
2000	1.530	0.070	23	3.2×10^{-6}	1×10^{-6}	4.2×10
			5	1.6×10^{-5}	4.9×10^{-6}	2.1×10
2500	1.530	0.030	23	3.0×10^{-6}	5.0×10^{-7}	3.5×10
			5	1.5×10^{-5}	2.4×10^{-6}	1.7×10
3000	1.530	0.008	23	2.8×10^{-6}	2.0×10^{-7}	3.0×10
			5	1.4×10^{-5}	9.8×10^{-7}	1.5×10

TABLE 5: Index of Refraction and Interaction Coefficients for AFCRL's Aerosol Models (14)

Rayleigh particles (gaseous molecules) and Mie particles (aerosols) are tabulated in Table 6. The coefficients for the composite (Rayleigh plus Mie) Model along with the corresponding value for the single scatter albedo are tabulated in Table 7. The single scatter albedo is defined as:

$$\overline{\omega} = \frac{K_S}{k} = \frac{K_S}{K_S + K_A}$$

The above data on aerosols applies for relative humidity values of less than 0.7. In Section 2 it was noted that the uptake of water by hydroscopic substances increased their size distribution. It also causes the complex index of refraction ($m = n - in'$) to vary between the dry aerosol value ($n \simeq 1.53$) and that of water ($n \simeq 1.34$). Both changes dramatically effect the interaction coefficients and the phase function.

Wavelength	Rayleigh Particles (Gaseous Molecules)			Visual Range	Mie Particles (Aerosols)		
(Å)	K_S (cm^{-1})	K_A (cm^{-1})	K (cm^{-1})	(K_m)	K_S (cm^{-1})	K_A (cm^{-1})	K(cm^{-1})
2000	$9.54x10^{-6}$	$7.17x10^{-5}$	$8.12x10^{-5}$	23	$3.2x10^{-6}$	$1x10^{-6}$	$4.2x10^{-}$
				5	$1.6x10^{-5}$	$4.9x10^{-6}$	$2.1x10^{-}$
2500	$3.38x10^{-6}$	$7.86x10^{-6}$	$1.12x10^{-5}$	23	$3.0x10^{-6}$	$5.0x10^{-7}$	$3.5x10^{-}$
				5	$1.5x10^{-6}$	$2.4x10^{-6}$	$1.7x10^{-}$
3000	$1.53x10^{-6}$	$2.41x10^{-7}$	$1.76x10^{-6}$	23	$2.8x10^{-6}$	$2.0x10^{-7}$	$3.0x10^{-}$
				5	$1.4x10^{-5}$	$9.8x10^{-7}$	$1.5x10^{-}$

TABLE 6: Composite Model - Interaction Coefficients for Rayleigh and Mie Particles

Wavelength (Å)	Visual Range (Km)	K_S (cm^{-1})	K_A (cm^{-1})	K (cm^{-1})	Single Scatter Albedo ω
2000	23	1.3×10^{-5}	7.3×10^{-5}	8.6×10^{-5}	0.15
	5	2.6×10^{-5}	7.7×10^{-5}	1.0×10^{-4}	0.26
2500	23	6.4×10^{-6}	8.4×10^{-6}	1.5×10^{-5}	0.43
	5	1.8×10^{-5}	1.0×10^{-5}	2.8×10^{-5}	0.64
3000	23	4.3×10^{-6}	4.4×10^{-7}	4.7×10^{-6}	0.92
	5	1.6×10^{-5}	1.2×10^{-6}	1.7×10^{-5}	0.94

TABLE 7: Composite Model - Values for the Interaction Coefficients and the Single Scatter Albedo

References

1. G.V. Rosenberg, "Optical Investigation of Atmospheric Aerosol," Soviet Physics Uspekhi, Vol. II, No. 3, Nov-Dec, 1968.

2. H.C. Hottel and A.F. Sarofim, Radiative Transfer, McGraw Hill, 1967.

3. H.C. VanDeHulst, Light Scattering By Small Particles, J. Wiley & Sons, 1957.

4. R. Penndorf, "Tables of the Refractive Index for Standard Air and the Rayleigh Scattering Coefficient for the Spectral Region between 0.2 and 20.0μm and Their Application to Atmospheric Optics," Journal of the Optical Society, Vol. 47, No. 2, February 1957.

5. R.M. Goody, Atmospheric Radiation, I Theoretical Basis, Oxford 1964.

6. R.D. Hudson, "Critical Review of Ultraviolet Photoabsorption Cross-Section for Molecules of Astrophysical and Aeronomic Interest," NSRDS-NBS 38, Issued August 1971.

7. D. Deirmendjian, Electromagnetic Scattering On Spherical Polydispersions, Elsevier 1969.

8. J.V. Dave, "Subroutines For Computing The Parameters of The Electromagnetic Radiation Scattered by a Sphere," 360D-17.4. 002, IBM Corporation, Program Information Department, 40 Shaw Mill River Road, Hawthorne, New York 10532.

9. J.V. Dave, "Effect of Coarseness of the Integration Increment on the Calculation of The Radiation Scattered by Polydispersed Aerosols," Applied Optics, Vol. III, No. 6, June 1969.

10. J.V. Dave, "Effect of Varying Integration Increment on The Computed Polarization Characteristics of the Radiation Scattered by Polydispersed Aerosols," Applied Optics, Vol. 8, No. 10, October 1969.

11. A.J. LaRocca and R.E. Turner, Atmospheric Transmittance and Radiance, Methods of Calculation, Environmental Research Institute of Michigan, June 1975.

References, continued

12. R.E. Danielson, D.R. Moore and H.C. VanDeHulst, "The Transfer of Visible Radiation Through Clouds," Journal of The Atmospheric Sciences, Vol. 26. Pg. 1078, September 1969.

13. M. Born and E. Wolf, Principles of Optics, Third (Revised) Edition, Pergamon Press, 1965.

14. R.A. McClatchey and J.E.A. Selby, "Atmospheric Attenuation of Laser Radiation From 0.76 to 31.25μ," 3 January 1974 AFCRL-TR-74-0003.

SECTION 4 - PROPAGATION

---

1. INTRODUCTION

The propagation of electromagnetic energy from a transmitter to a receiver through a medium involves interactions of various types and degrees with the constituents. In the case of propagation through the atmosphere the constituents are gaseous molecules and suspended and precipitating matter. Due to variations in the number densities and size distributions of the constituents (varying meteorological conditions), the variations in the magnitude and temporal characteristics of the received signals are dramatic. The suspended (aerosol) and precipitating particles are the most

variable constituents and the principal effect of increasing their number **density** and size distribution is to increase the amount of energy in the scatter field. For the spectral region of interest, scattering from aerosols is predominantly in the forward direction (i.e., greater than 95% of the scattered energy is scattered into the forward hemisphere).

If energy received from the scatter field is viewed as potentially useful signal energy, then the variations in signal amplitude (ΔE) may be reduced by increasing signal reception time (Δt). Based on the above it seems reasonable to characterize the atmosphere by some constant product of reception time and signal amplitude variations; i.e.,

$$\Delta E \, \Delta t = \text{constant}$$

This implies that the dynamic range of signal amplitude (ΔE) may be maintained below a given value if the reception time (Δt) is made sufficiently large. (Reception time is inversely proportional to bandwidth.) The constant is determined by wavelength, distance between the transmitter and receiver and transmission and reception geometry.

Signal amplitude (E_R) is a function of the intensity of the primary and scatter fields and time; i.e.,

$$E_R(t) = \int_{\Delta t} \left[H_p(t) + H_s(t) \right] dt$$

where: H_p and H_s are the intensities of the primary and scatter fields respectively.

The primary field intensity is readily determined from knowledge of the extinction coefficient which characterizes the medium and will be discussed in Part 2. The scatter field intensity may be the result of transmitted photons which have undergone one or more scattering interactions enroute to the receiver. When the ratio of multiple to single scattered photons is small a condition of single scattering may be declared. In Part 3 a theoretical model for determining the temporal response of the atmosphere under conditions of signle scattering is proposed, developed and applied for various types of scattering and transmission and reception geometries. In Part 4 the extinction and single scatter model will be used to determine the propagation characteristics in the middle ultraviolet for the atmospheric models developed in Section 3.

2. EXTINCTION MODEL

It was noted in the introduction that the radiation field at the receiver would be the sum of the primary and scatter fields. It is desired to determine the magnitude, and variations in magnitude of the primary field as a result of changing meteorological conditions. This information will then be utilized to establish the relative importance of the scatter field once its magnitude has been ascertained.

The magnitude of the primary field may be determined from the Bouger - Lambert Extinction Law and geometry. The Extinction Law for a collimated beam is:

$$\frac{dI}{I} = -K d\ell$$

where: $k = k_s + k_A$ = extinction coefficient

$$\therefore \quad I = I_o e^{-k\ell} \quad \text{Watts/cm}^2$$

For a diverging beam the geometric factors plus the Extinction Law give the following expression for the primary power density at the receiver:

$$H_p = \frac{P_T}{\Omega} \frac{e^{-k\ell}}{\ell^2} \quad \frac{\text{Watts}}{\text{cm}^2} \qquad (1)$$

where: P_T = Total power transmitted

Ω = Solid angle of radiation cone

ℓ = Distance from transmitter to receiver

k = Extinction coefficient which characterizes the medium

e^{-kx} = Ratio of that which arrives in the presence of a medium to that which would arrive in a vacuum

If a pulse is transmitted, the received pulse will be delayed in time and reduced in amplitude but will retain its original shape. Hence, all the energy will be received during a time established by the pulse width of the transmitted pulse.

In practice, primary plus scattered energy will be received where the magnitude of the received scattered energy will be a function of the interaction coefficients and phase functions which characterize the medium and receiver and transmitter geometry (distance between receiver and transmitter, radiation and reception cones and collection interval). Zuev[1] and his coworkers have investigated the dependencies of the above parameters for various media. They express the received intensity (from a collimated beam) as:

$$I_R = I_o e^{-\tau} + I_o \tau e^{-\tau} D$$

$$= \text{primary} + \text{scattered}$$

where: $\tau = kx$ = optical depth

$$D = \frac{1}{2} \int_o^{\psi} \int_o^{\theta} f(\psi+\theta)\cos\psi \, d\psi \, d\theta$$

ψ = aperture angle of receiver

θ = cone angle of point source

$f(\psi+\theta)$ = normalized phase function

This relation implies that the ratio of scatter to primary radiation is:

$$\frac{I_s}{I_p} = \tau D$$

Therefore, for small optical depths and small radiation and reception geometries this is a relatively small number. Typical numbers

for small optical depths ($\tau < 2$) are 10^{-3}-10^{-4} [1]. The effects of receiver field-of-view have also been investigated by Stewart and Curcio[2], and Gumprecht[3].

Therefore, the magnitude of the primary field may be determined analytically or experimentally. Analytically, it is defined by equation (1); experimentally, the measured value must be corrected for the contribution due to scattered energy.

3. SINGLE SCATTER MODEL

When the scattered radiation field at the receiver is primarily established by radiation resulting from single scattering events; i.e., transmitted photons which undergo only one coherent scattering interaction before arriving at the receiver, a single scatter model may be utilized to determine the intensity of the scattered radiation for various atmospheric and system configurations. Such a model is developed in this section and adapted to various types of scattering.

The criteria for utilizing a single scatter model is that the "optical scattering depth" between the transmitter and receiver is less than 0.3[4]. The "optical scattering depth" is defined to be equal to $K_s X$ or X/λ_s where K_s is the total scattering coefficient (Rayleigh plus Mie scattering coefficients), X is the physical path length and λ_s is the scattering mean free path.

The model is based upon a fundamental property of the prolate spheroid (an ellipse which has been rotated about its major axis) which states that the distance between the foci and any point on the surface of a prolate spheroid is a constant, or in other words, the sum of the focal radii is constant for a given surface. This property, plus the fact that the speed of light in the medium is a constant, allows one to think of a surface as an "equi-temporal scattering surface" since scattered radiation from all points on the surface which is the result of an impulse transmitted isotropically from one focal point (trans-

mitter focal point) will arrive at the other focal point (receiver focal point) at the same time.

The object of the model is to develop an expression for the intensity of the scattered radiation at the receiving focal point versus time due to an impulse transmitted at t=0, in terms of transmitter, receiver and atmospheric parameters. The amount of scattered energy collected by a receiver with a 1 cm^2 collecting are will then be the integral of the intensity over the collection interval.

(a) General Scattering Model: The basic geometry for the following step-by-step development of the model is shown in Figure 1. The transmitter is positioned at one focal point and the receiver at the other. The prolate spheroidal coordinate system is utilized since the "equi-temporal scattering surfaces" are constants in this system, and the mathematics become more tractable. The coordinate system is discussed in Appendix 1.

The basic approach involves developing an expression for the energy scattered from a differential volume dV located at a point $P(\xi, \eta, \phi)$, dividing by the differential time dt associated with scattering from dV to obtain an average intensity, and finally to take the limit as the radial component ($d\xi$) of dV approaches zero to obtain the instantaneous intensity. The total instantaneous intensity is obtained by integrating over the surface (over η and ϕ).

Before proceeding with the development of the model, expressions must be derived for several variables ($r_1, r_2, \theta_1, \theta_2$ and θ_s) in terms of the prolate spheroidal coordinates (ξ, η, ϕ) and the interfocal distance ℓ.

- Focal Radii (r_1 & r_2): The focal radii are the directed lines between the focal points (F_1 & F_2) and the point $P(\xi, \eta, \phi)$ on the surface of a prolate spheroid. F_1: $P(\xi, \eta, \phi)$ defines the transmitter focal radius (r_1) and F_2: $P(\xi, \eta, \phi)$ defines the receiver focal radius (r_2).

$$r_1^2 = x^2 + (z+\ell/2)^2; \quad r_2^2 = x^2 + (\ell/2-z)^2$$

$$r_1^2 - r_2^2 = (r_1+r_2)(r_1-r_2) = 2z\ell$$

but $r_1 + r_2 = \ell\xi$ (length of major axis)

$$\Rightarrow r_1 - r_2 = \frac{2z}{\xi}; \quad r_2 = r_1 - \frac{2z}{\xi}$$

$$r_1 = \ell\xi - r_2 = \ell\xi - r_1 + \frac{2z}{\xi}$$

$$\Rightarrow r_1 = \frac{1}{2}\left(\ell\xi + \frac{2z}{\xi}\right)$$

since $z = \frac{\ell}{2}\eta\xi$

$$\therefore \boxed{\begin{aligned} r_1 &= \frac{\ell}{2}(\xi+\eta) \\ r_2 &= \frac{\ell}{2}(\xi-\eta) \end{aligned}}$$

Note: $r_1 + r_2 = \ell\xi$; $r_1 - r_2 = \ell\eta$

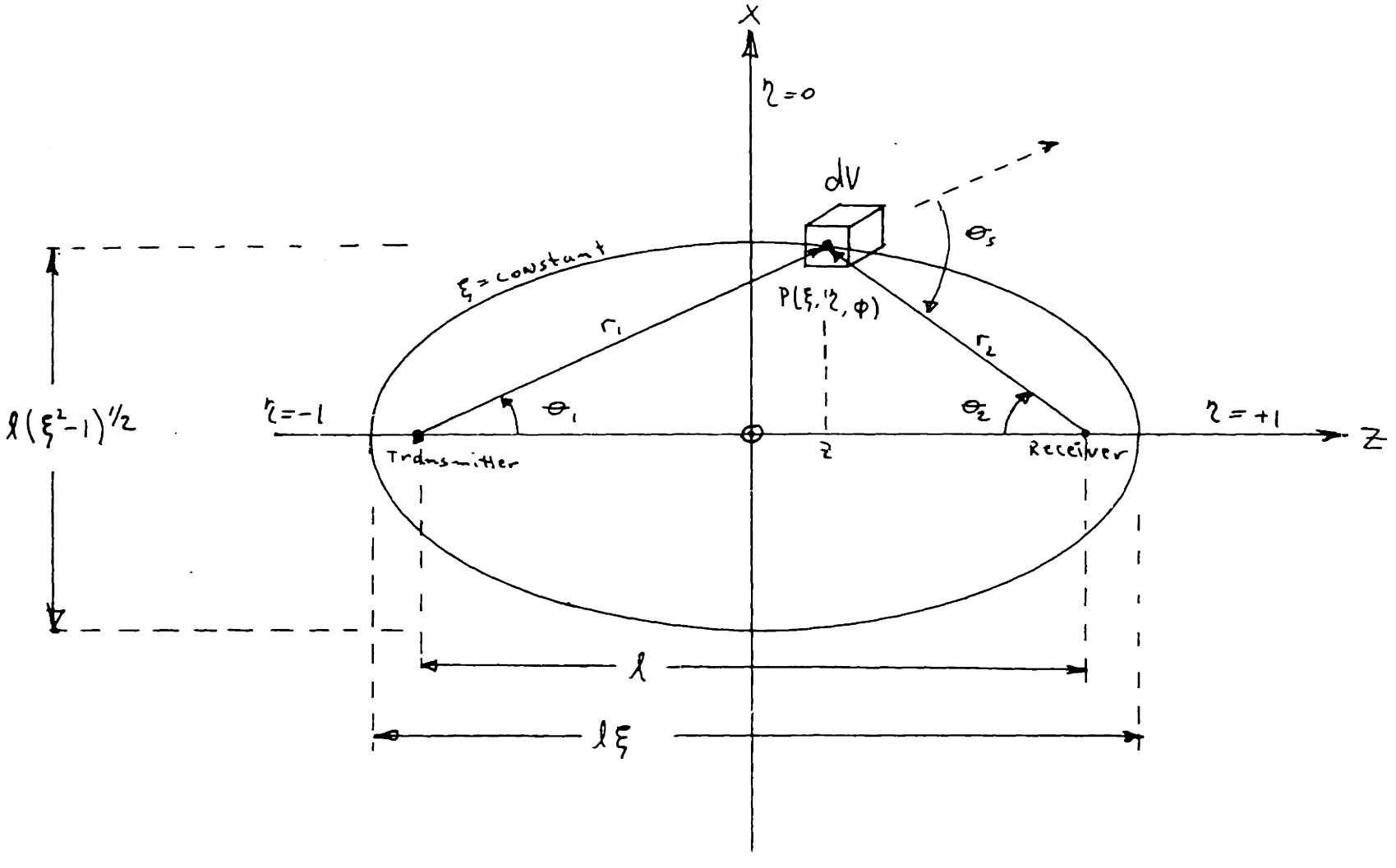

Figure 1 - Basic Scattering Geometry

- Focal Angles (θ_1 & θ_2): The angles defined by the focal radii, the focal points, and the interfocal axis are called the focal angles. θ_1 refers to the transmitter focal point F_1, and θ_2 refers to the receiver focal point F_2.

$$r_2^2 = \ell^2 + r_1^2 - 2\ell r_1 \cos\theta_1$$

$$r_1^2 = \ell^2 + r_2^2 - 2\ell r_2 \cos\theta_2$$

$$\Rightarrow \cos\theta_1 = \frac{\ell^2 - (r_2^2 - r_1^2)}{2\ell r_1} \; ; \; \cos\theta_2 = \frac{\ell^2 + (r_2^2 - r_1^2)}{2\ell r_2}$$

$$r_2^2 - r_1^2 = (r_2+r_1)(r_2-r_1) = (\ell\xi)(-\ell\eta) = -\ell^2\xi\eta$$

$$\boxed{\theta_1 = \cos^{-1}\left(\frac{1+\xi\eta}{\xi+\eta}\right)}$$

$$\boxed{\theta_2 = \cos^{-1}\left(\frac{1-\xi\eta}{\xi-\eta}\right)}$$

$$0 \le \theta_1 \le \pi; \; 0 \le \theta_2 \le \pi$$

- Scattering Angle (θ_s): The scattering angle (θ_s) is defined by the forward direction of the incident radiation (extension of r_1), the scattering point $P(\xi, \eta, \phi)$ and the direction of observation (r_2) as shown in Figure 2.

$$\theta_s + (\pi - \theta_1 - \theta_2) = \pi$$

$$\Rightarrow \theta_s = \theta_1 + \theta_2$$

$$\cos\theta_s = \cos(\theta_1+\theta_2) = \cos\theta_1 \cos\theta_2 - \sin\theta_1 \sin\theta_2$$

$$\sin\theta_1 = \left[1 - \cos^2\theta_1\right]^{1/2} = \frac{(\xi^2+\eta^2-1-\xi^2\eta^2)^{1/2}}{\xi+\eta}$$

$$\sin\theta_2 = \left[1 - \cos^2\theta_2\right]^{1/2} = \frac{(\xi^2+\eta^2-1-\xi^2\eta^2)^{1/2}}{\xi-\eta}$$

$$\Rightarrow \sin\theta_1 \sin\theta_2 = \frac{(\xi^2+\eta^2-1-\xi^2\eta^2)^{1/2}}{(\xi+\eta)(\xi-\eta)}$$

$$\cos\theta_1 \cos\theta_2 = \frac{(1-\xi^2\eta^2)}{(\xi+\eta)(\xi-\eta)}$$

$$\cos\theta_s = \frac{2 - \xi^2 - \eta^2}{\xi^2-\eta^2}$$

$$\therefore \boxed{\theta_s = \cos^{-1}\left(\frac{2 - \xi^2 - \eta^2}{\xi^2-\eta^2}\right)}$$

Figure 2 is a plot of θ_s versus η with ξ as the parameter. The following conclusions may be drawn from this figure:

(i) $0^\circ \leq \theta_s \leq 180^\circ$

(ii) The function is symmetric with respect to $\eta=0$.

(iii) θ_{smin} for a given ξ is at $\eta=0$.

(iv) θ_s approaches 180° as ξ approaches infinity (prolate spheroidal approaches a sphere).

(v) θ_s approaches 0° as ξ approaches 1 (prolate spheroid approaches a straight line).

(vi) θ_s is always 180° for $\eta=\pm 1$.

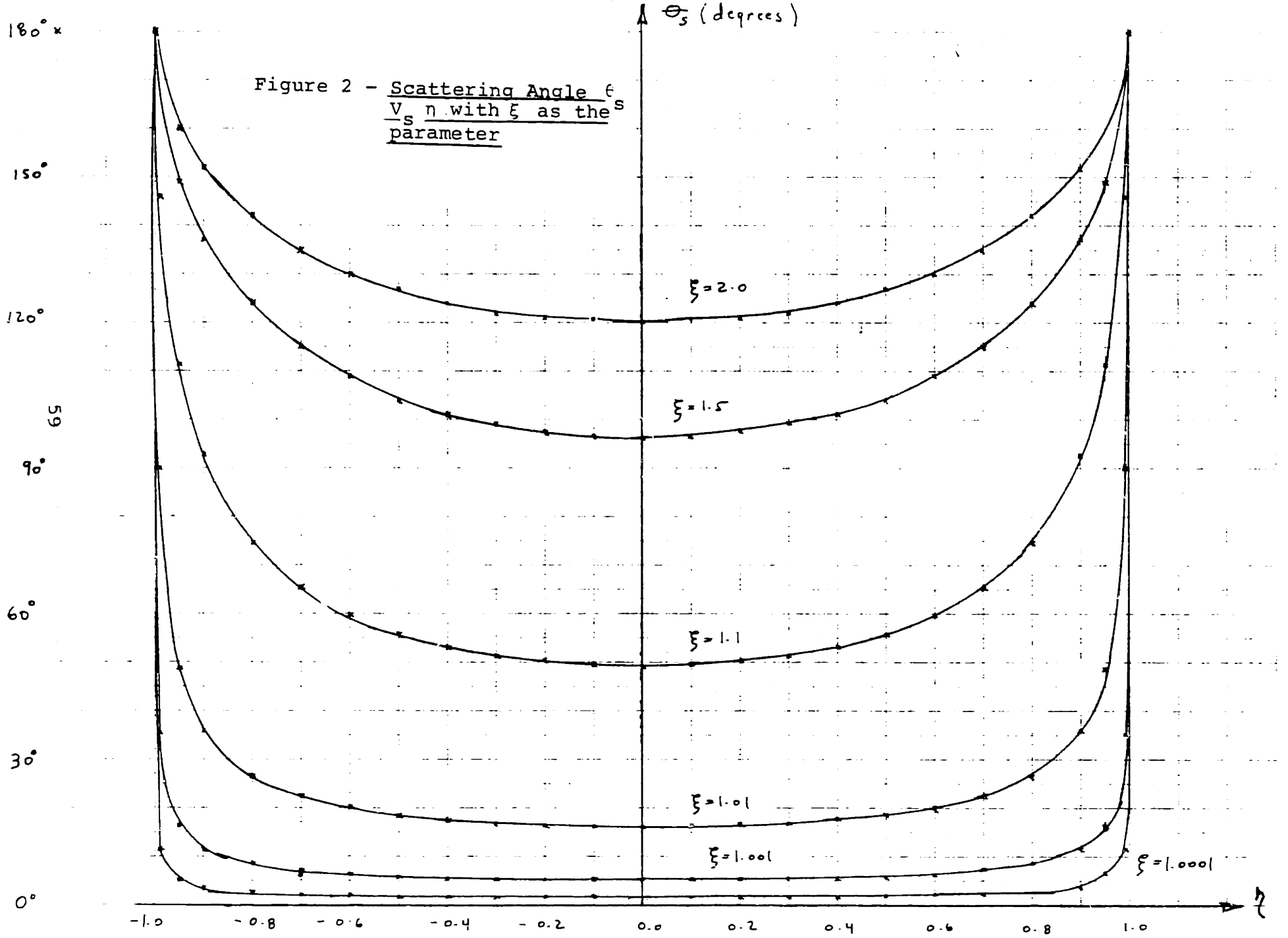

Figure 2 - Scattering Angle θ_s Vs η with ξ as the parameter

The step-by-step development of the general model proceeds as follows: (See Figure 1).

(1) At t=0 an impulse of energy of magnitude E_T leaves the transmitter focal point;

$$E_T \qquad \text{Joules}$$

(2) The energy transmitted per unit solid angle is obtained by dividing the total transmitted energy (E_T) by the solid angle of the transmitted beam (Ω);

$$\frac{E_T}{\Omega} \qquad \frac{\text{Joules}}{\text{sr}}$$

(3) At point $P(\xi, \eta, \phi)$, a distance r_1 from the transmitter, the following density is experienced at time $t = \frac{r_1}{c}$;

$$\frac{E_T}{\Omega} \frac{e^{-kr_1}}{r_1^2} \qquad \frac{\text{Joules}}{\text{cm}^2}$$

where:
- k is the extinction coefficient associated with the medium through which the energy has propagated.
- e^{-kr_1} is the ratio of the energy which arrives to that which would arrive if the intervening medium were a vacuum.

Note: The above density may also be thought of as being proportional to the number of photons crossing a 1 cm^2 area located at $P(\xi, \eta, \phi)$ at time $t = \frac{r_1}{c}$

(4) Due to scattering from the differential volume located at $P(\xi, \eta, \phi)$ a secondary source is established;

$$\left[\frac{E_T}{\Omega} \frac{e^{-kr_1}}{r_1^2}\right] \frac{k_s}{4\pi} p(\cos\theta_s) dV \qquad \text{Joules/sr}$$

The step-by-step development of the general model proceeds as follows: (See Figure 1).

(1) At t=0 an impulse of energy of magnitude E_T leaves the transmitter focal point;

$$E_T \qquad \text{Joules}$$

(2) The energy transmitted per unit solid angle is obtained by dividing the total transmitted energy (E_T) by the solid angle of the transmitted beam (Ω);

$$\frac{E_T}{\Omega} \qquad \frac{\text{Joules}}{\text{sr}}$$

(3) At point $P(\xi, \eta, \phi)$, a distance r_1 from the transmitter, the following density is experienced at time $t = \frac{r_1}{c}$;

$$\frac{E_T}{\Omega} \frac{e^{-kr_1}}{r_1^2} \qquad \frac{\text{Joules}}{\text{cm}^2}$$

where:
- k is the extinction coefficient associated with the medium through which the energy has propagated.
- e^{-kr_1} is the ratio of the energy which arrives to that which would arrive if the intervening medium were a vacuum.

Note: The above density may also be thought of as being proportional to the number of photons crossing a 1 cm^2 area located at $P(\xi, \eta, \phi)$ at time $t = \frac{r_1}{c}$

(4) Due to scattering from the differential volume located at $P(\xi, \eta, \phi)$ a secondary source is established;

$$\left[\frac{E_T}{\Omega} \frac{e^{-kr_1}}{r_1^2}\right] \frac{k_s}{4\pi} p(\cos\theta_s) dV \qquad \text{Joules/sr}$$

where:
- k_s is the scattering coefficient per cm associated with the medium.
- $p(\cos\theta_s)$ is the single scatter phase function as defined in Section 3.

Note: This secondary source is a result of an impulse interacting with a medium while transiting through it. The interaction or transit time for the scattering volume dV is dr_1/c.

(5) Some of the energy from the secondary source (scattering in dV) will propagate in the direction of the receiver focal point;

$$\left[\frac{E_T}{\Omega}\ \frac{e^{-kr_1}}{r_1^2}\right]\left[\frac{k_s}{4\pi}\ p(\cos\theta_s)dV\right]\ \frac{e^{-kr_1}}{r_2^2} \qquad \text{Joules/cm}^2$$

$$= \frac{E_T}{4\pi\Omega}\ \frac{e^{-k(r_1+r_2)}}{r_1^2 r_2^2}\ p(\cos\theta_s)dV \qquad \text{Joules/cm}^2$$

(6) Rewriting the above expression in terms of the prolate spheroidal coordinates ξ, η and ϕ and the interfocal distance ℓ;

$$r_1 = \frac{\ell}{2}(\xi+\eta)\ ;\ r_2 = \frac{\ell}{2}(\xi-\eta)$$

$$r_1 + r_2 = \ell\xi\ ;\ r_1^2 r_2^2 = \frac{\ell^4}{2}\ (\xi^2-\eta^2)^2$$

$$dV = \frac{\ell}{2}^3\ (\xi^2-\eta^2)\,d\xi\,d\eta\,d\phi$$

$$\frac{E_T K_s}{4\pi\Omega} \frac{e^{-k\ell\xi}}{(\ell/2)(\xi^2-\eta^2)} p(\cos\theta_s)\, d\xi\, d\eta d\phi \quad \text{Joules/cm}^2$$

where: $p(\cos\theta_s)$ is still an unspecified function

(7) Due to the radial component ($d\xi$) of dV a differential transmission time (dt) is associated with the secondary source (i.e., the secondary source is not impulsive). Dividing the above expression by dt results in an average intensity at the receiver focal point;

$$\bar{H}_s'(\xi,\eta,\phi) = \frac{E_T k_s}{4\pi\Omega} \frac{e^{-k\ell\xi}}{(\ell/2)(\xi^2-\eta^2)} p(\cos\theta_s) \frac{d\xi\, d\eta d\phi}{dt} \frac{\text{Watts}}{\text{cm}^2}$$

(8) Expressing $d\xi$ in terms of dt ($d\xi = cdt/\ell$) and taking the limit as dt approaches zero leads to the instantaneous intensity;

$$H_s'(\xi,\eta,\phi) = \frac{CE_T k_s}{2\pi\Omega\ell^2} \frac{e^{-k\ell\xi}}{(\xi^2-\eta^2)} p(\cos\theta_s)\, d\phi d\eta \frac{\text{Watts}}{\text{cm}^2}$$

(9) Integration over ϕ and η provides the scattered intensity at the receiver focal point due to the entire surface;

$$H_s(\xi,\eta,\phi) = \frac{CE_T k_s e^{-k\ell\xi}}{2\pi\Omega\ell^2} \int_{\eta_1}^{\eta_2} \int_{\phi=0}^{2\pi} \frac{p(\cos\theta_s)}{(\xi^2-\eta^2)}\, d\phi d\eta \frac{\text{Watts}}{\text{cm}^2}$$

(10) Since the integrand is not a function of the azimuth coordinate (ϕ) the above expression reduces to;

$$H_s(\xi,\eta) = \frac{CE_T k_s}{\Omega \ell^2} e^{-k\ell\xi} \int_{\eta_2}^{\eta_2} \frac{p(\cos\theta_s)}{(\xi^2-\eta^2)} d\eta \quad \frac{\text{Watts}}{\text{cm}^2}$$

(11) Limits of integration for η: When the transmitter and receiver are isotropic (transmitter beam solid angle = 4πSr and receiver field-of-view = 4πSr), integration takes place over the entire prolate spheriodal surface ξ = constant (i.e., $\eta_1 = -1$ and $\eta_2 = +1$). However, for all other radiation and reception geometries integration will be required over a partial surface (see Figure 3). Since the problem is symmetrical with respect to the major axis (azimutal symmetry), only the limits for the angular component (η) will be effected. Again, referring to Figure 3, it may be concluded that both limits are a function of ξ and that η_1 is a function of θ_1 and η_2 is a function of θ_2. It is therefore necessary to derive general expressions for η_1 and η_2 in terms of θ_1, θ_2 and ξ.

let θ_{1max} = 1/2 cone angle of the transmitter beam.

let θ_{2max} = 1/2 angle of the receiver field-of-view.

$$\cos\theta_{1max} = \left(\frac{1+\xi\eta_1}{\xi+\eta_1}\right)$$

$$\Rightarrow \xi\cos\theta_{1max} + \eta_1\cos\theta_{1max} = 1 + \xi\eta_1$$

$$\therefore \eta_1 = \frac{\xi \cos \theta_{1max} - 1}{\xi - \cos \theta}$$

$$\cos \theta_{2max} = \left(\frac{1 - \xi \eta_2}{\xi - \eta_2} \right)$$

$$\Rightarrow \xi \cos \theta_{2max} - \eta_2 \cos \theta_{2max} = 1 - \xi \eta_2$$

$$\therefore \eta_2 = \frac{1 - \xi \cos \theta_{2max}}{\xi - \cos \theta_{2max}}$$

Since η_1 is dependent on transmitter radiation geometry and η_2 is dependent on reception geometry, it is probably appropriate to let $\eta_1 = \eta_{xmtr}$ and $\eta_2 = \eta_{rcvr}$.

$$\eta_{xmtr}(\xi, \theta_{1max}) = \frac{\xi \cos \theta_{1max} - 1}{\xi - \cos \theta_{1max}}$$

$$\eta_{rcvr}(\xi, \theta_{2max}) = \frac{1 - \xi \cos \theta_{2max}}{\xi - \cos \theta_{2max}}$$

(12) Finally, the expression for the scattered intensity at the receiving focal point;

$$H_s(\xi) = \frac{CE_T k_s}{\Omega \ell^2} e^{-k\ell\xi} \int_{\eta_{xmtr}}^{\eta_{rcvr}} \frac{p(\cos \theta_s)}{(\xi^2 - \eta^2)} d\eta \quad \frac{\text{Watts}}{\text{cm}^2} \qquad (2)$$

where: Ω = solid angle of the transmitted beam

$= 2\pi (1 - \cos \theta_{2max})$

(13) For closed radiation and reception geometries ($\theta_{1max} + \theta_{2max} < \pi$) there exists a finite maximum value for the radial component and a finite scattering volume.

a) Maximum Value of Radial Component (ξ_{max}): Since ξ is the ratio of the scattered path length to the direct path length (interfocal distance), ξ_{max} will establish a finite time interval during which scattered energy may be received. At ξ_{max}, $\eta_{xmtr} = \eta_{rcvr}$ (see Figure 4);

$$\frac{\xi_{max} \cos \theta_{1max} - 1}{\xi_{max} - \cos \theta_{1max}} = \frac{1 - \xi_{max} \cos \theta_{2max}}{\xi_{max} - \cos \theta_{2max}}$$

$$(\xi_{max} - \cos \theta_{2max})(\xi_{max} \cos \theta_{1max})$$
$$= (1 - \xi_{max} \cos \theta_{2max})(\xi_{max} - \cos \theta_{1max})$$

$$\xi^2_{max} - 2\left(\frac{1 + \cos \theta_{1max} \cos \theta_{2max}}{\cos \theta_{1max} + \cos \theta_{2max}}\right)\xi_{max} + 1 = 0$$

$$\xi_{max} = \left(\frac{1 + \cos \theta_{1max} \cos \theta_{2max}}{\cos \theta_{1max} + \cos \theta_{2max}}\right) + \sqrt{\left(\frac{1 + \cos \theta_{1max} \cos \theta_{2max}}{\cos \theta_{1max} + \cos \theta_{2max}}\right)^2 - 1}$$

b) Finite Scattering Volume $(Vol)_s$: The scattering volume to be considered is the sum of two circular cones (see Figure 4);

$$(Vol)_s = \text{Vol. } 1 + \text{Vol. } 2$$

$$\text{Vol. } 1 = \frac{\pi}{3}\left(\frac{\ell}{2}\right)^2\left(\xi^2_{max} - 1\right)\left[\left(\frac{\ell}{2}\right)\left(1 + \eta_e \xi_{max}\right)\right]$$

$$\text{Vol. } 2 = \frac{\pi}{3}\left(\frac{\ell}{2}\right)^2\left(\xi^2_{max} - 1\right)\left[\left(\frac{\ell}{2}\right)\left(1 - \eta_e \xi_{max}\right)\right]$$

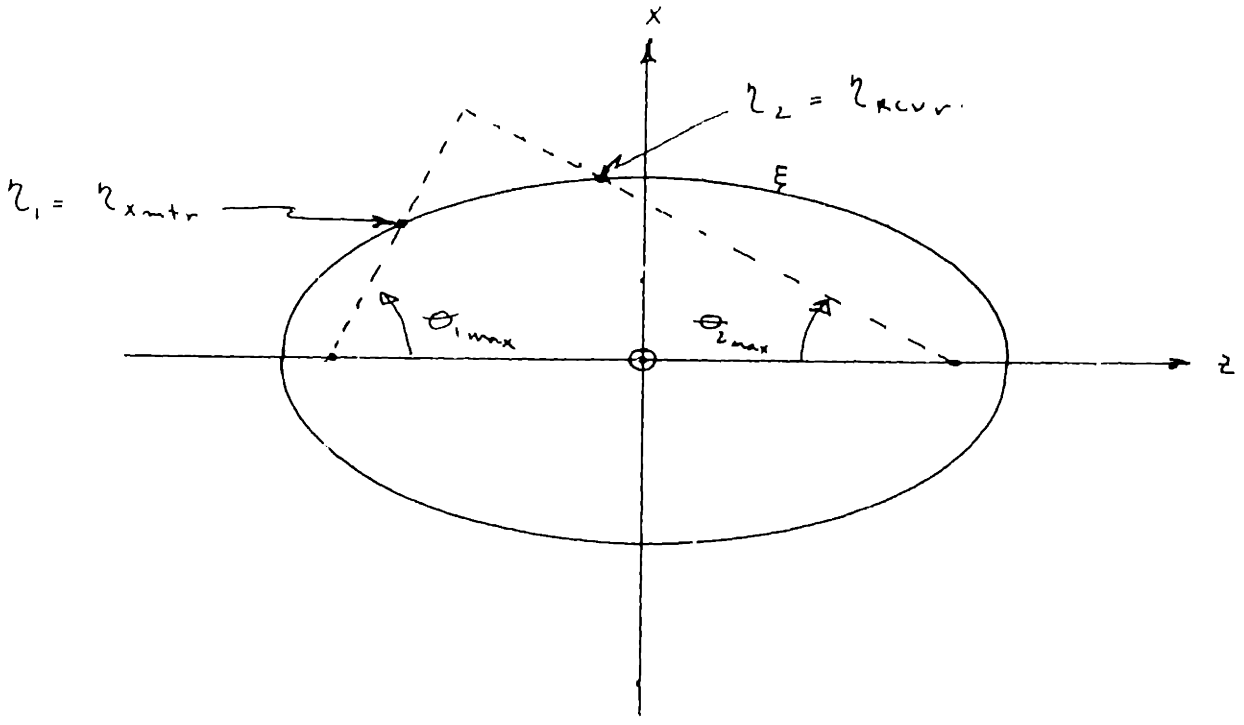

Figure 3 - Geometry for Determining Limits for η.

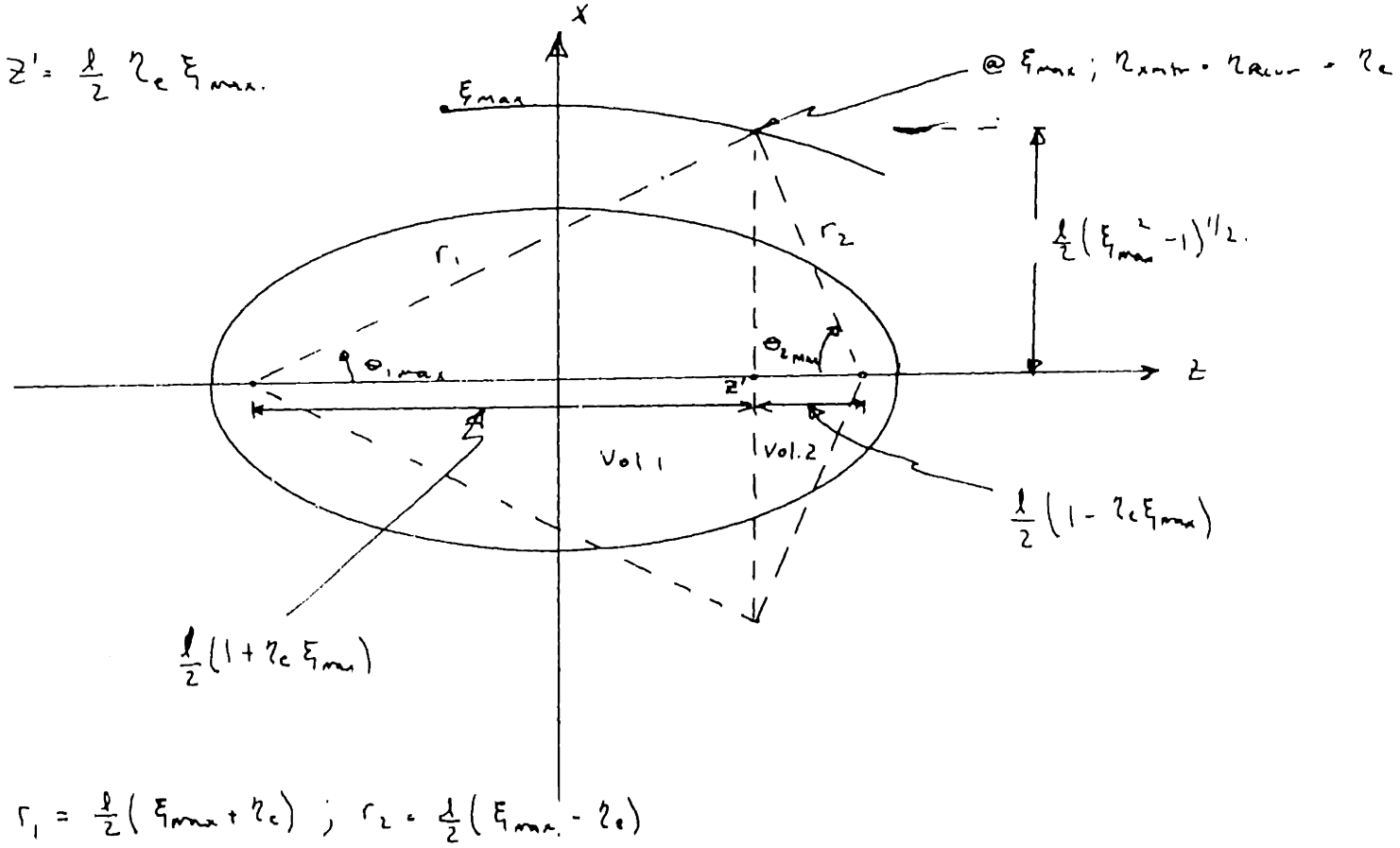

Figure 4 - Geometry for Determining ξ_{max} and $(Vol)_s$

$$\%\,(\mathrm{Vol})_s = \frac{2\pi}{3}\left(\frac{\ell}{2}\right)^3\left(\xi^2_{max} - 1\right)$$

(14) Temporal Transformations: The sum of the focal radii is constant for any point on the surface of a prolate spheroid. In a medium characterized by a constant propagation velocity, this implies that the transit time for photons traveling from one focal point to the other via scattering events on the surface is constant for any given surface. Therefore, ξ may be thought of as the ratio of the scattered-to-direct path lengths or scattered-to-direct transit times; i.e.,

$$\xi = \frac{r_1 + r_2}{\ell} = \frac{t^*}{t_o}$$

where: $r_1 + r_2$ = scattered path length

ℓ = direct path length

$t^* = \frac{r_1 + r_2}{c}$ = transit time for scattered photons

$t_o = \frac{\ell}{c}$ = transit time for photons which proceed directly to the receiver

It may be observed that since ξ is defined for values greater than or equal to one ($1 \leq \xi < \infty$) that t^* can only take on values greater than or equal to t_o ($t_o \leq t^* < \infty$). Now $H(\xi)$ may be transformed into the following time dependent expression:

$$H(t^*) = \frac{CE_T k_s}{\Omega \ell^2} e^{-ckt^*} \int_{\eta_{xmtr}}^{\eta_{rcvr}} \frac{p(\cos\theta_s)}{\left[\left(\frac{c}{\ell}t^*\right)^2 - \eta^2\right]} d\eta \quad \frac{\text{Watts}}{\text{cm}^2}$$

$$t_o \leq t^* \leq \infty; \; t_o = \ell/c$$

Since it is desired to characterize the temporal characteristics of the scattered radiation, and since $H_s(t^*)$ is zero for all time less than or equal to t_o, a new variable (t_s) is defined as follows:

$$t_s = t^* - t_o$$

where: $o \leq t_s < \infty$

$t_o = \ell/c$

All data and graphs will be in terms of t_s. Expressions will be developed in subsequent paragraphs for the intensity when the single scatter phase functions are specified. To keep the expressions as simple as possible, they will be written in terms of ξ instead of t_s.

b) Isotropic Scattering Model:

$$H_s(\xi) = \frac{CE_T k_s}{\Omega \ell^2} e^{-k\ell\xi} \int_{\eta_{xmtr}}^{\eta_{rcvr}} \frac{p(\cos\theta_s)}{(\xi^2 - \eta^2)} d\eta \quad \frac{\text{Watts}}{\text{cm}^2} \qquad (2)$$

where: $p(\cos\theta_s) = 1$

$$\Omega = 2\pi(1 - \cos\theta_{1max})$$

$$\eta_{rcvr} = \frac{1 - \xi \cos\theta_{2max}}{\xi - \cos\theta_{2max}}$$

$$\eta_{xmtr} = \frac{\xi \cos \theta_{1max} - 1}{\xi - \cos \theta_{1max}}$$

$$\int_{\eta_{xmtr}}^{\eta_{rcvr}} \frac{p(\cos\theta_s)}{(\xi^2-\eta^2)}\, d\eta = \int_{\eta_{xmtr}}^{\eta_{rcvr}} \frac{1}{(\xi^2-\eta^2)}\, d\eta$$

$$= \frac{1}{2\xi} \ln\left[\left(\frac{\xi + \eta_{rcvr}}{\xi - \eta_{rcvr}}\right)\left(\frac{\xi - \eta_{xmtr}}{\xi + \eta_{xmtr}}\right)\right]$$

$$H_s(\xi) = \frac{CE_T k_s}{2\Omega \ell^2} \frac{e^{-k\ell\xi}}{\xi} \ln\left[\left(\frac{\xi + \eta_{rcvr}}{\xi - \eta_{rcvr}}\right)\left(\frac{\xi - \eta_{xmtr}}{\xi + \eta_{xmtr}}\right)\right] \quad \frac{\text{Watts}}{\text{cm}^2}$$

Since η_{rcvr} and η_{xmtr} are expressible in terms of the variable ξ and the parameters cos θ_{1max} and cos θ_{2max}, a more physical expression for $H(\xi)$ is obtained by substitution;

$$\therefore H_s(\xi) = \frac{CE_T k_s}{2\Omega \ell^2} \frac{e^{-k\ell\xi}}{\xi} \ln\left[\frac{(\xi^2 - 2\xi \cos\theta_{2max} + 1)(\xi^2 - 2\xi \cos\theta_{1max} + 1)}{(\xi^2-1)^2}\right]$$

Watts cm^{-2}

Special Radiation and Reception Geometries

(i) 4π Sr Transmitter and Receiver (Isotropic Transmitter and Receiver)

$$\Rightarrow \theta_{1max} = \theta_{2max} = \pi$$

$$\Omega = 4\pi \text{ Sr}$$

$$\therefore H_s(\xi) = \frac{CE_T k_s}{4\pi \ell^2} \frac{e^{-k\ell\xi}}{\xi} \ln\left[\frac{\xi + 1}{\xi - 1}\right] \quad \frac{\text{Watts}}{\text{cm}^2}$$

(ii) 4π Sr Transmitter and 2π Sr Receiver

$$\Rightarrow \theta_{1max} = \pi;\ \theta_{2max} = \pi/2$$

$$\Omega = 4\pi \text{ Sr}$$

$$H_s(\xi) = \frac{CE_T k_s}{8\pi \ell^2} \frac{e^{-k\ell\xi}}{\xi} \ell n\left[\frac{(\xi^2+1)}{(\xi+1)^2}\right] \quad \frac{\text{Watts}}{\text{cm}^2}$$

(iii) 2 Sr Transmitter and Receiver

$$\theta_{1max} = \theta_{2max} = \pi/2$$

$$\Omega = 2\pi \text{ Sr}$$

$$H(\xi) = \frac{CE_T k_s}{2\pi \ell^2} \frac{e^{-k\ell\xi}}{\xi} \ell n\left[\frac{(\xi^2+1)}{(\xi^2-1)}\right] \quad \frac{\text{Watts}}{\text{cm}^2}$$

The intensity $H_s(t_s)$ and collected energy $E_s(t_s)$, (the integral of $H_s(t_s)$) have been computed as a function of t_s for several atmospheric and system configuration.

(a) Effects of Absorption by the Atmosphere: The intensity and collected energy were first calculated for a conservative atmosphere ($\bar{\omega} = 1.0 \Rightarrow k_A = 0$), and then for the case where the absorption and scattering coefficients were equal ($\bar{\omega} = 0.5$). k_s for both cases was 1.5×10^{-6} cm^{-1}. The two cases are shown in Figure 5. It may be concluded that the effect of absorption is a reduction in intensity and collected energy where the magnitude of the reduction is exponential with time (i.e., k_A increases the value of the argument in exponential terms in equation (2)).

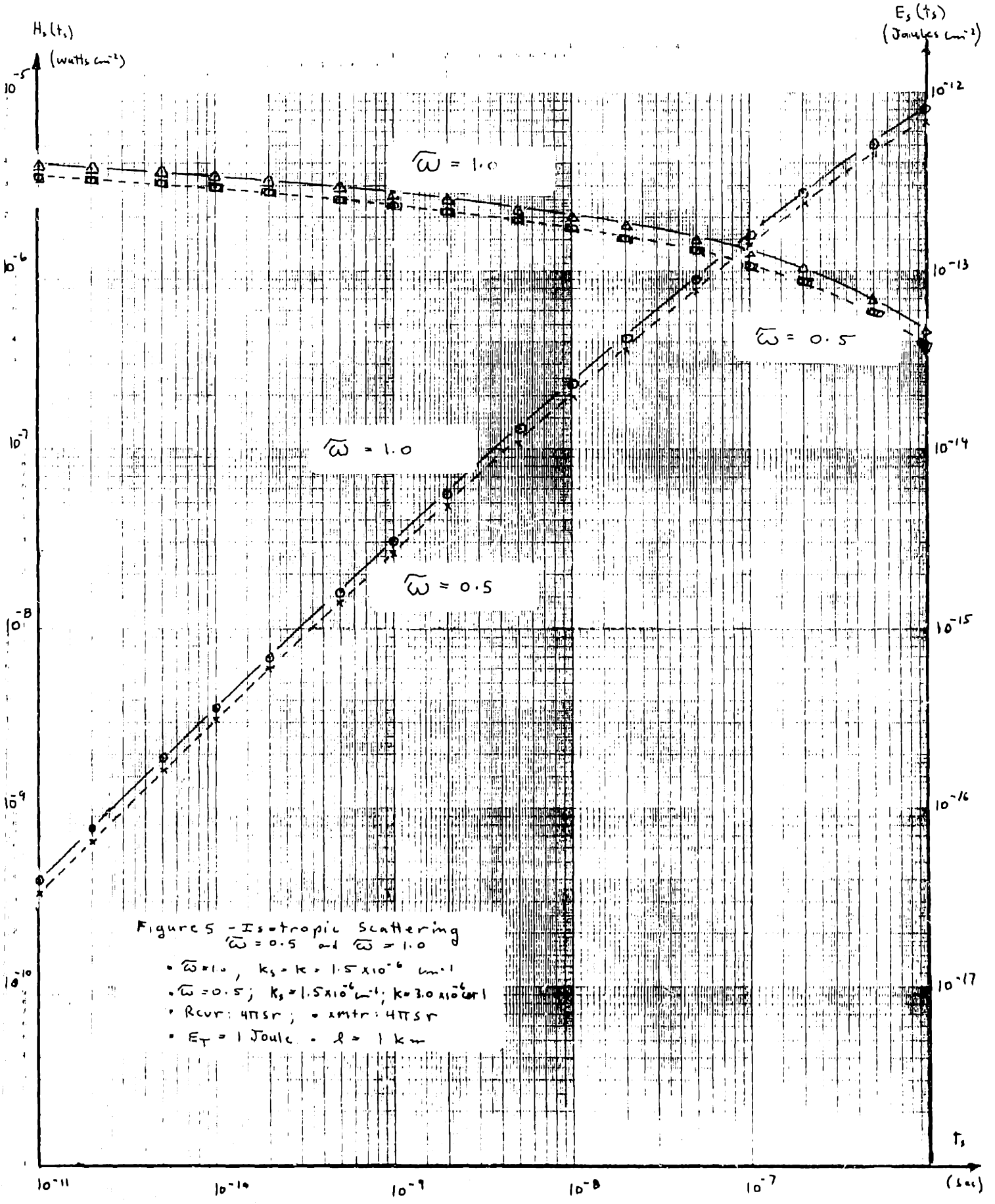

Figure 5 - Isotropic Scattering
$\tilde{\omega} = 0.5$ and $\tilde{\omega} = 1.0$

- $\tilde{\omega} = 1.0$, $k_s = k = 1.5 \times 10^{-6}$ cm^{-1}
- $\tilde{\omega} = 0.5$; $k_s = 1.5 \times 10^{-6}$ cm^{-1}; $k = 3.0 \times 10^{-6}$ cm^{-1}
- Rcvr: 4π sr ; • xmtr: 4π sr
- E_T = 1 Joule • ℓ = 1 km

(b) Effects of Transmission and Reception Geometry:

The intensities and collected energy were evaluated for three configurations of transmission and reception geometry (i.e., solid angle of the transmitted beam and F.O.V. of the receiver). The energy transmitted was the same for each case. It may be concluded from Figure 6 that the effect of reducing the geometry is to decrease the interval required to collect a given amount of scattered energy. Also note that if a "large" collection interval (inversely proportional to bandwidth) may be tolerated, then the 4π Sr case is superior for isotropic scattering.

(c) Effects of Range: The 4π Sr configuration was evaluated at three different ranges (0.25 Km, 0.50 Km and 1.00 Km). It may be concluded from Figure 7 that the effect of increasing range is to reduce the magnitude and rate of change of $H_s(t_s)$.

c) Rayleigh Scattering Model:

$$H_s(\xi) = \frac{CE_T k_s}{\Omega \ell^2} e^{-k\ell\xi} \int_{\eta_{xmtr}}^{\eta_{rcvr}} \frac{p(\cos\theta_s)}{(\xi^2 - \eta^2)} d\eta \quad \frac{\text{Watts}}{\text{cm}^2} \qquad (2)$$

where: $p(\cos\theta_s) = \frac{3}{4}(1 + \cos^2\theta_s)$

$$\Omega = 2\pi(1 - \cos\theta_{1max})$$

$$\eta_{rcvr} = \frac{1 - \xi\cos\theta_{2max}}{\xi - \cos\theta_{2max}}$$

$$\eta_{xmtr} = \frac{\xi\cos\theta_{1max} - 1}{\xi - \cos\theta_{1max}}$$

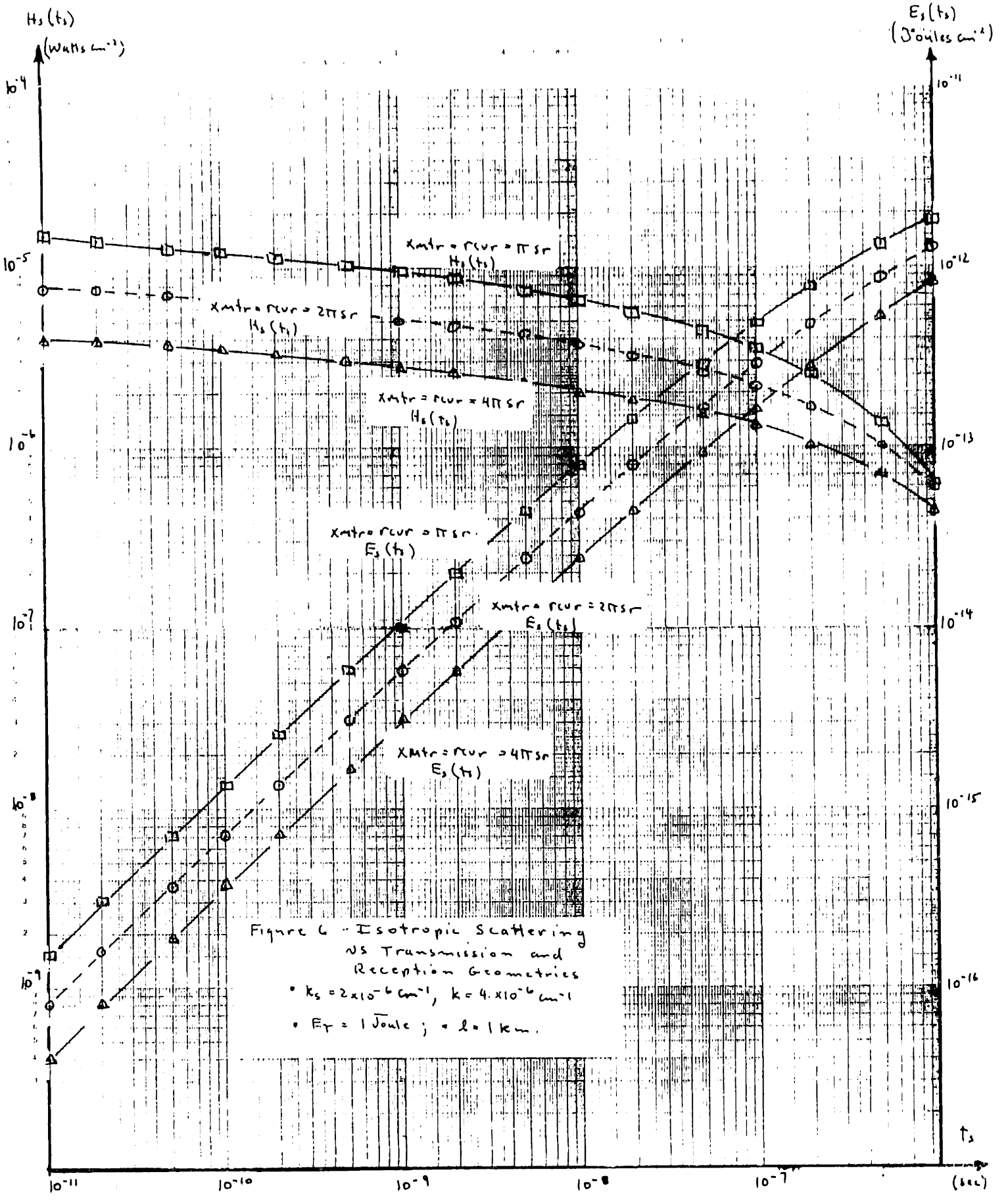

Figure 6 - Isotropic Scattering vs Transmission and Reception Geometries

- $k_s = 2 \times 10^{-6}$ cm^{-1}, $k = 4. \times 10^{-6}$ cm^{-1}
- E_T = 1 Joule ; ℓ = 1 km.

THE FOLLOWING PAGES ARE PARTIALLY ILLEGIBLE

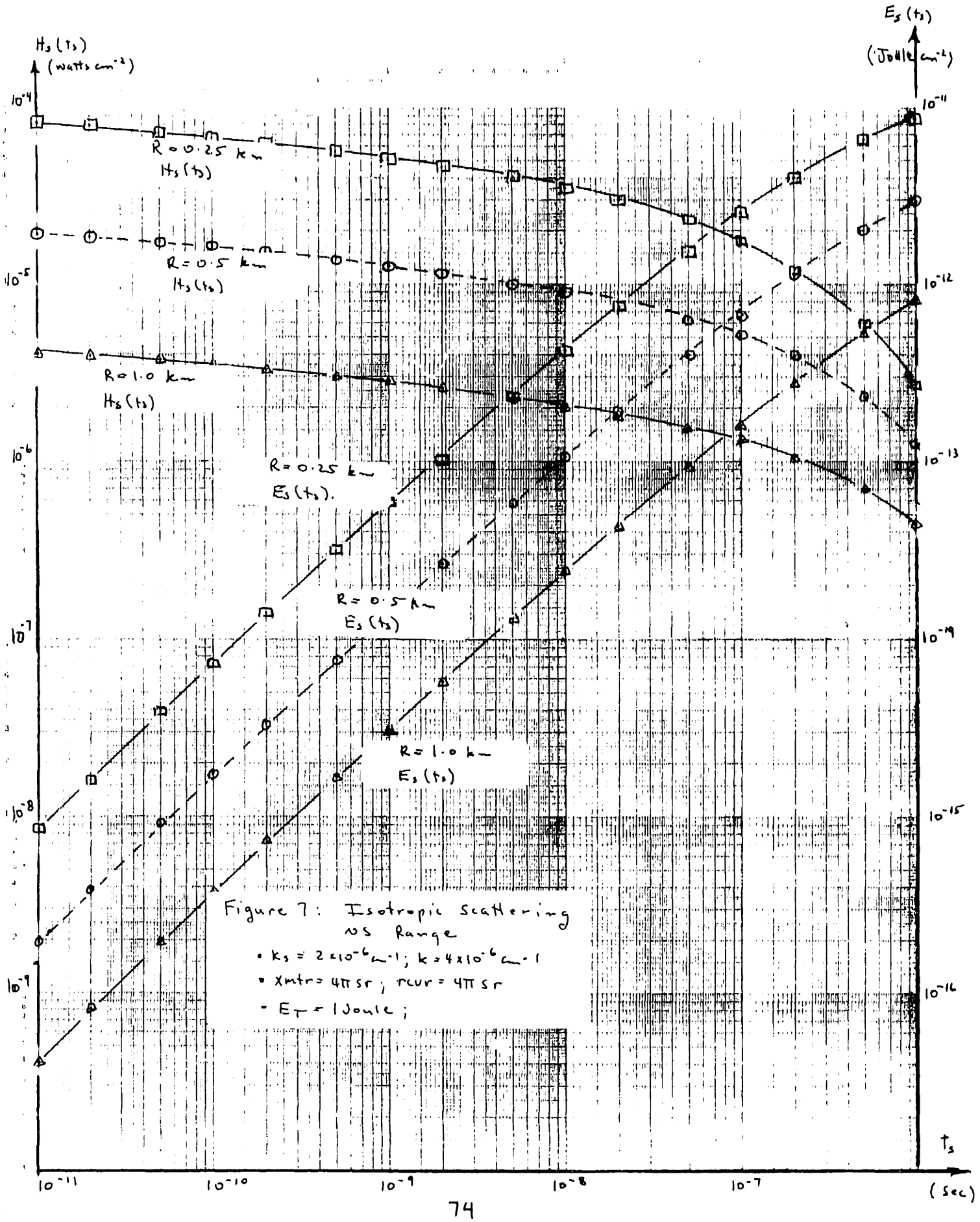

Figure 7: Isotropic Scattering vs Range

- $k_s = 2 \times 10^{-6}$ cm^{-1}; $k = 4 \times 10^{-6}$ cm^{-1}
- Xmtr = 4π sr ; rcvr = 4π sr
- E_T = 1 Joule ;

THE FOLLOWING PAGES ARE PARTIALLY ILLEGIBLE

$$\cos\theta_s = \frac{2 - \xi^2 - \eta^2}{\xi^2 - \eta^2}$$

$$\int_{\eta_{xmtr}}^{\eta_{rcvr}} \frac{p(\cos\theta_s)}{(\xi^2-\eta^2)}\, d\eta = \frac{3}{4} \int_{\eta_{xmtr}}^{\eta_{rcvr}} \frac{(1+\cos^2\theta_s)}{\xi^2 - \eta^2}\, d\eta$$

$$\cos^2\theta_s = \frac{\eta^4 + (2\xi^2-4)\eta^2 + (\xi^4-4\xi^2+4)}{\left(\xi^2-\eta^2\right)^2}$$

$$\Rightarrow \int_{\eta_{xmtr}}^{\eta_{rcvr}} \frac{p(\cos\theta_s)}{\xi^2 - \eta^2}\, d\eta = \frac{3}{4}\left[\int_{\eta_{xmtr}}^{\eta_{rcvr}} \frac{1}{\xi^2 - \eta^2}\, d\eta + \int_{\eta_{xmtr}}^{\eta_{rcvr}} \frac{\eta^4}{\left(\xi^2-\eta^2\right)^3}\, d\eta \right.$$

$$\left. + (2\xi^2-4) \int_{\eta_{xmtr}}^{\eta_{rcvr}} \frac{\eta^2}{\left(\xi^2-\eta^2\right)^3}\, d\eta + (\xi^4-4\xi^2+4) \int_{\eta_{xmtr}}^{\eta_{rcvr}} \frac{1}{\left(\xi^2-\eta^2\right)^3}\, d\eta \right]$$

Note: See Appendix 2 for evaluation of the above integrals.

$$= 3/4 \left[\frac{1}{2\xi} \ln\left(\frac{\xi+\eta}{\xi-\eta}\right) - \frac{5\eta}{8(\xi^2-\eta^2)} + \frac{3}{16\xi} \ln\left(\frac{\xi+\eta}{\xi-\eta}\right) \right.$$

$$+ \frac{\xi^2\eta}{4(\xi^2-\eta^2)^2} + \frac{(2\xi^2-4)\eta}{4(\xi^2-\eta^2)^2} - \frac{(2\xi^2-4)\eta}{8\xi^2(\xi^2-\eta^2)}$$

$$- \frac{(2\xi^2-4)}{16\xi^3} \ln\left(\frac{\xi+\eta}{\xi-\eta}\right) + \frac{(\xi^4-4\xi^2+4)\eta}{4\xi^2(\xi^2-\eta^2)^2}$$

$$\left. + \frac{3(\xi^4-4\xi^2+4)\eta}{8^4(\xi^2-\eta^2)} + \frac{3(\xi^4-4\xi^2+4)}{16\xi^5} \ln\left(\frac{\xi+\eta}{\xi-\eta}\right) \right]$$

$$= \frac{3}{4\xi^2} \left[\frac{(3\xi^4-2\xi^2+3)}{4\xi^3} \ln\left(\frac{\xi+\eta}{\xi-\eta}\right) \right.$$

$$\left. - \frac{(\xi^4+2\xi^2-3)\eta}{2\xi^2(\xi^2-\eta^2)} + \frac{(\xi^4-2\xi^2+1)\eta}{(\xi^2-\eta^2)^2} \right]$$

$$\rightarrow H_s(\xi) = \frac{3C\,E_T\,k_s}{4\Omega\ell^2} \frac{e^{-k\ell\xi}}{\xi^2} \left[\frac{3\xi^4-2\xi^2+3)}{4\xi^3} \ln\left(\frac{\xi+\eta}{\xi-\eta}\right) \right.$$

$$\left. - \frac{(\xi^4+2\xi^2-3)\eta}{2\xi^2(\xi^2-\eta^2)} + \frac{(\xi^4-2\xi^2+1)\eta}{(\xi^2-\eta^2)^2} \right]_{\eta_{XMTR}}^{\eta_{RCVR}}$$

$$\underset{\infty}{} H_s(\xi) = \frac{3c\ E_T\ k_s}{4\Omega\ell^2} \frac{e^{-k\ell\xi}}{\xi^2} \left[\frac{(3\xi^4 - 2\xi^2+3)}{4\ \xi^3} \right.$$

$$\ell\eta \left[\frac{(\xi + \eta_{RCVR})(\xi - \eta_{xmtr})}{(\xi - \eta_{RCVR})(\xi + \eta_{xmtr})} \right]$$

$$- \frac{(\xi^4 + 2\xi^2 - 3)}{2\ \xi^2} \left[\frac{\eta_{RCVR}}{(\xi^2 - \eta^2_{RCVR})} - \frac{\eta_{xmtr}}{(\xi^2 - \eta^2_{xmtr})} \right]$$

$$+ \frac{(\xi^4 - 2\xi^2 + 1)}{1} \left. \left[\frac{\eta_{RCVR}}{(\xi^2 - \eta^2_{RCVR})^2} - \frac{\eta_{xmtr}}{(\xi^2 - \eta^2_{xmtr})^2} \right] \right]$$

watts cm^{-2}

Special Radiation and Reception Geometries

(i) 4π sr Transmitter and Receiver (Isotropic transmitter and receiver)

$$\Theta_{1max} = \Theta_{2max} = \pi$$

$$\Omega = 4\pi \text{ sr}$$

$$H_s(\xi) = \frac{3c\ E_T\ k_s}{16\pi\ell^2} \frac{e^{-k\ell\xi}}{\xi^2} \left[\frac{(3\xi^4 - 2\xi^2 + 3)}{2\ \xi^3} \ell n \left(\frac{\xi + 1}{\xi - 1} \right) \right.$$

$$\left. - \frac{(\xi^4 + 2\xi^2 - 3)}{\xi^2\ (\xi^2 - 1)} + \frac{2(\xi^4 - 2\xi^2 + 1)}{(\xi^2 - 1)^2} \right] \frac{\text{watts}}{cm^2}$$

$$H_s(\xi) = \frac{3CE_T k_s}{16\pi \ell^2} \frac{e^{-k\ell\xi}}{\xi^2} \left[\frac{(3\xi^4 - 2\xi^2 + 3)}{2\xi^3} \ell n \left(\frac{\xi + 1}{\xi - 1} \right) - \frac{(\xi^2+3)}{\xi^2} + 2 \right] \quad \frac{\text{Watts}}{\text{cm}^2}$$

(ii) 4π Sr Transmitter and 2π Sr Receiver

$\Rightarrow \theta_{1max} = \pi; \quad \theta_{2max} = \pi/2$

$\Omega = 4\pi$ Sr

$$H_s(\xi) = \frac{3CE_T k_s}{16\pi \ell^2} \frac{e^{-k\ell\xi}}{\xi^2} \left[\frac{(3^4 - 2\xi^2 + 3)}{4\xi^2} \ell n \left[\frac{(\xi^2+1)}{(\xi+1)} \right] - \frac{(\xi^2+3)}{2\xi^2} \frac{(\xi^2+\xi+1)}{(\xi^2+1)} + \frac{(\xi^4+\xi^3+2\xi^2+2)}{\left(\xi^2+1\right)^2} \right] \quad \frac{\text{Watts}}{\text{cm}^2}$$

(iii) 2π Sr Transmitter and Receiver

$\Rightarrow \theta_{1max} = \theta_{2max} = \pi/2$

$\Omega = 2\pi$

$$H_s(\xi) = \frac{3CE_T k_s}{8\pi \ell^2} \frac{e^{-k\ell\xi}}{\xi^2} \left[\frac{(3\xi^4 - 2\xi^2 + 3)}{2\xi^2} \ell n \left(\frac{\xi^2 + 1}{\xi^2 - 1} \right) - \frac{(\xi^2+3)}{\xi(\xi^2+1)} + \frac{2\xi^3}{\left(\xi^2+1\right)^2} \right] \quad \frac{\text{Watts}}{\text{cm}^2}$$

Irradiance and collected energy were calculated for the same cases as for Isotropic Scattering; the results are similar.

(d) Comparison Between Isotropic and Rayleigh Scattering:

Due to the nature of the Rayleigh and Isotropic phase functions (Section 3, Figure 1), one expects that the magnitude of Rayleigh scattering will predominate in the forward and backward directions and that Isotropic scattering will predominate for scattering angles (θ_s) between 60°-120°, Figure 2 shows the dependency of θ_s on ξ and η. It may be concluded that when the average scattering angle is $\simeq 60°$, that $\xi \simeq 1.1$ and when it is $\simeq 120°$, $\xi \simeq 1.6$. For an interfocal distance of 1 Km, this implies that isotropic scattering should predominate for 200 ns $\leq t_s \leq$ 2000 ns seconds. This is indeed the fact as may be observed on Figure 8.

(e) Mie Scattering Model:

Note: This is basically Mie Scattering where the single scatter phase function is approximated by the Henyey-Greenstein function.

$$H_s(\xi) = \frac{CE_T k_s}{\Omega \ell^2} e^{-k\ell\xi} \int_{\eta_{xmtr}}^{\eta_{rcvr}} \frac{p(\cos\theta_s)}{(\xi^2-\eta^2)} d\eta \quad \frac{\text{Watts}}{\text{cm}^2} \qquad (2)$$

where: $$p(\cos\theta_s) = \frac{1 - g^2}{\left(1 + g^2 - 2g\cos\theta_s\right)^{3/2}}$$

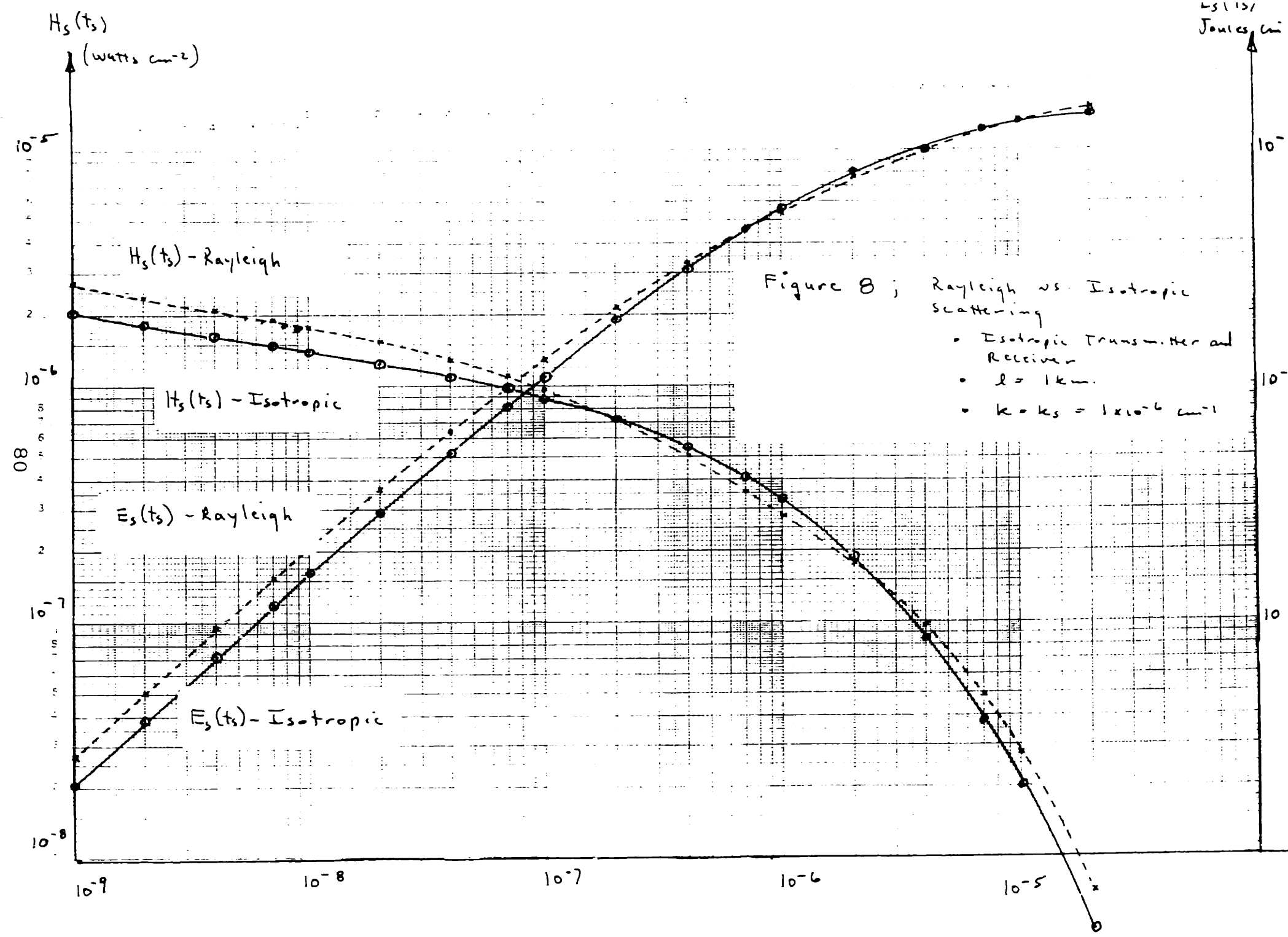

Figure 8 ; Rayleigh vs Isotropic scattering

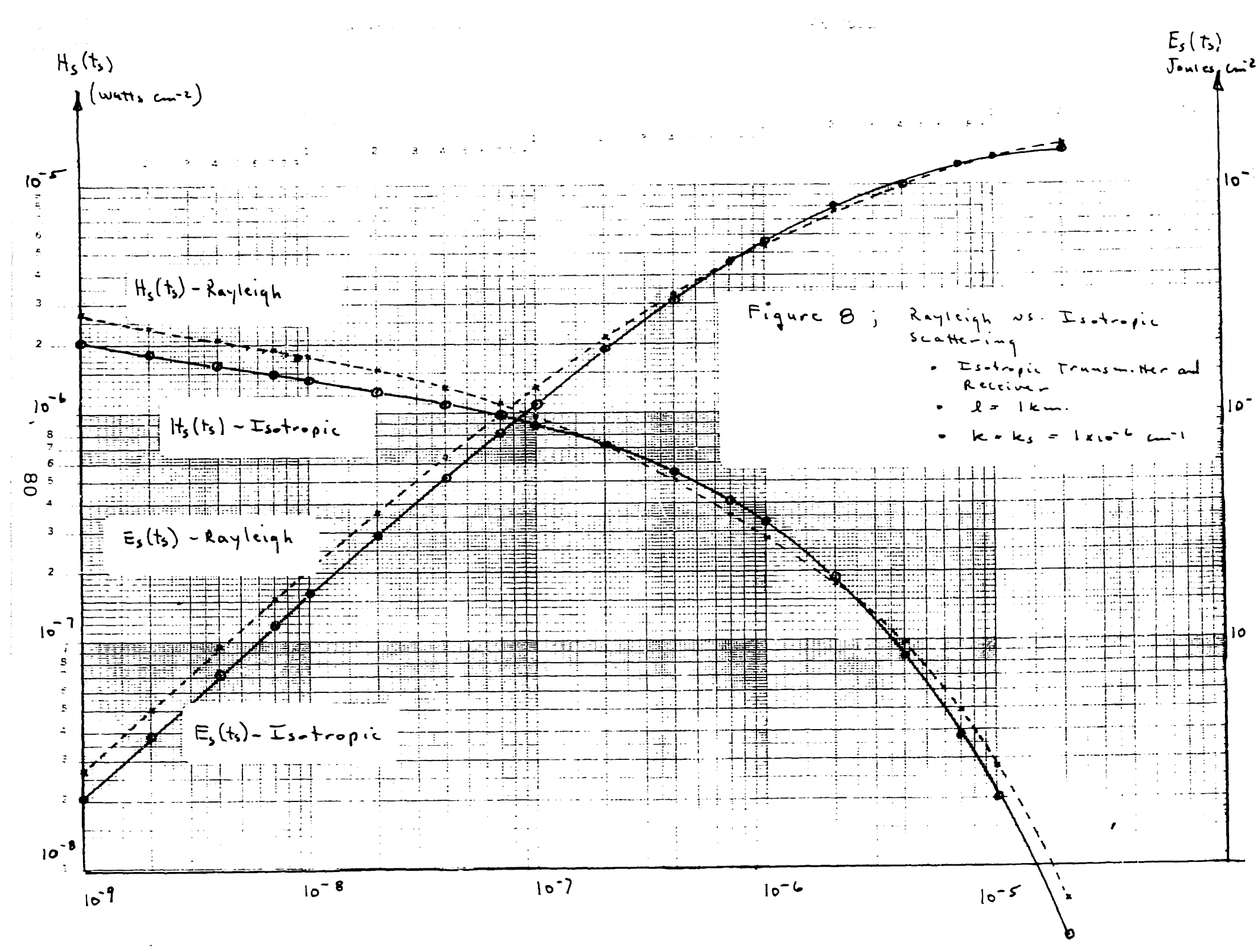

Figure 8 ; Rayleigh vs. Isotropic scattering

- Isotropic Transmitter and Receiver
- l = 1 km.
- $k = k_s = 1 \times 10^{-6}$ cm^{-1}

$$\cos\ \theta_s = \frac{2 - \xi^2 - \eta^2}{\xi^2 - \eta^2}$$

$$\Omega = 2\pi(1 - \cos\ \theta_{2max})$$

$$\eta_{rcvr} = \frac{1 - \xi\ \cos\ \theta_{2max}}{\xi - \cos\ \theta_{2max}}$$

$$\eta_{xmtr} = \frac{\xi\ \cos\ \theta_{1max} - 1}{\xi - \cos\ \theta_{1max}}$$

$$\int_{\eta_{xmtr}}^{\eta_{rcvr}} \frac{p(\cos\ \theta_s)}{(\xi^2-\eta^2)}\, d\eta = \int_{\eta_{xmtr}}^{\eta_{rcvr}} \frac{(1-g^2)}{\left(\xi^2-\eta^2\right)\left(1+g^2-2g\cos\theta_s\right)^{3/2}}\, d\eta$$

$$= (1-g^2) \int_{\eta_{xmtr}}^{\eta_{rcvr}} \frac{1}{(\xi^2-\eta^2)\left[1 + g^2 - 2g\left(\frac{2 - \xi^2 - \eta^2}{\xi^2 - \eta^2}\right)\right]^{3/2}}\, d\eta$$

$$= \frac{(1-g^2)}{\left(g^2-2g+1\right)^{3/2}} \int_{\eta_{xmtr}}^{\eta_{rcvr}} \frac{(\xi^2-\eta^2)^{1/2}}{\left[\frac{(g^2+2g+1)^2 - 4g\ \eta^2}{(g^2+2g+1)}\right]^{3/2}}\, d\eta$$

$$H_s(\xi) = \frac{CE_T k_s}{\Omega \ell^2} e^{-k\ell\xi} \frac{(1-g^2)}{\left(g^2-2g+1\right)^{3/2}}$$

$$\times \int_{\eta_{xmtr}}^{\eta_{rcvr}} \frac{(\xi^2-\eta^2)^{1/2}}{\left[\frac{(g^2+2g+1)\xi^2 - 4g}{(g^2-2g+1)} - \eta^2\right]^{3/2}} d\eta \quad \frac{\text{Watts}}{\text{cm}^2}$$

Notes: (1) $g = \overline{\cos \theta_s}$; $0 \leq g < 1$

(2) When $g = 0$, $H_s(\xi)$ reduces to the isotropic case.

(3) The integral is evaluated numerically by Gauss-Legendre 24 point integration.

For Mie Scattering, the magnitude of the scatter field at the receiver is strongly dependent on the anisotropy of the phase function. This fact is illustrated in Figures 9 and 10. Since the scattering is predominantly forward, it is expected that radiation and reception geometry will play a significant role in determining the amount of scattered energy collected. This dependency may be observed in Figures 11 and 12.

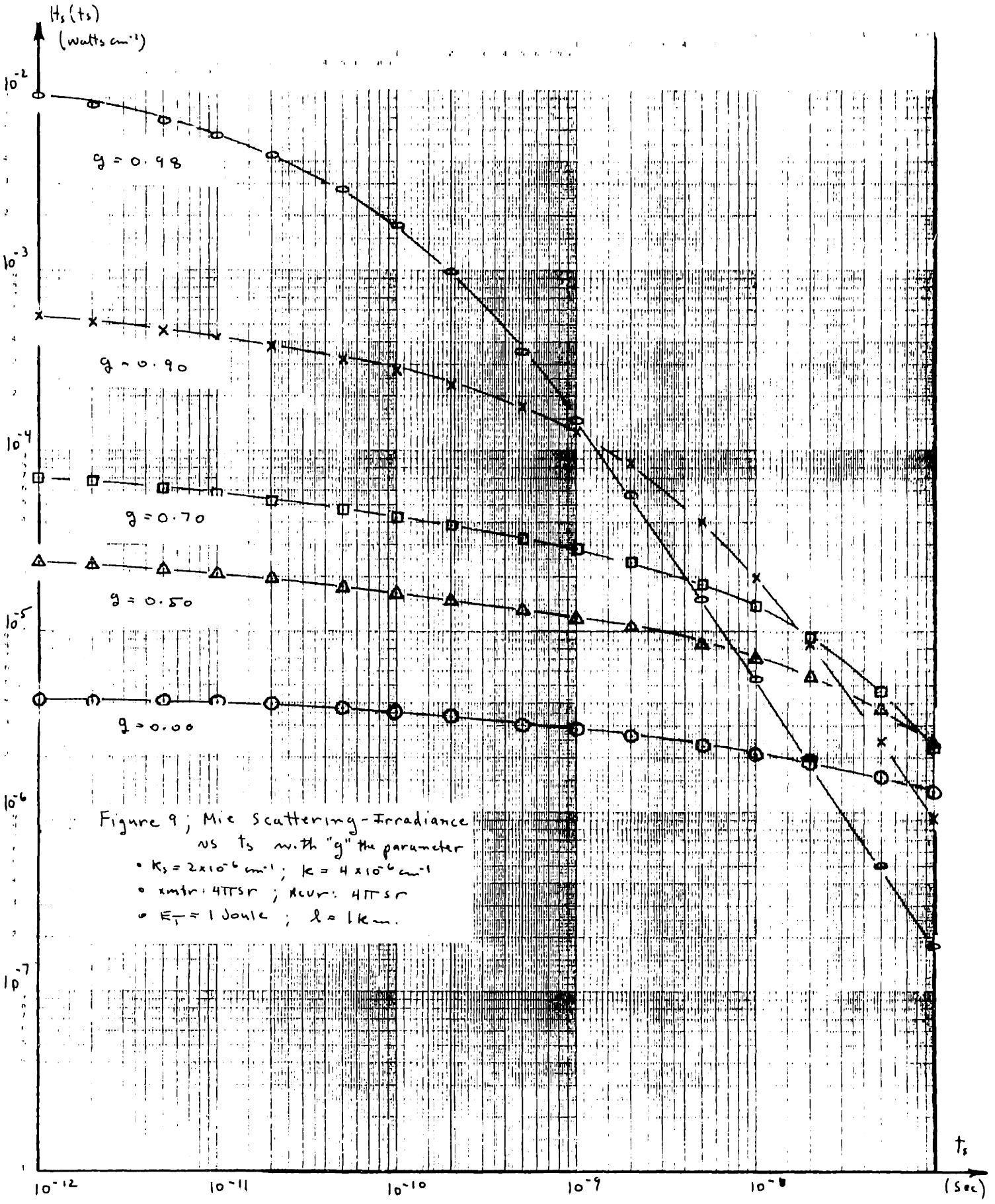

Figure 9; Mie Scattering - Irradiance vs t_s with "g" the parameter

- $K_s = 2 \times 10^{-6}$ cm^{-1}; $K = 4 \times 10^{-6}$ cm^{-1}
- xmtr: 4π sr; rcvr: 4π sr
- E_T = 1 Joule; l = 1 km.

THE FOLLOWING PAGES ARE PARTIALLY ILLEGIBLE

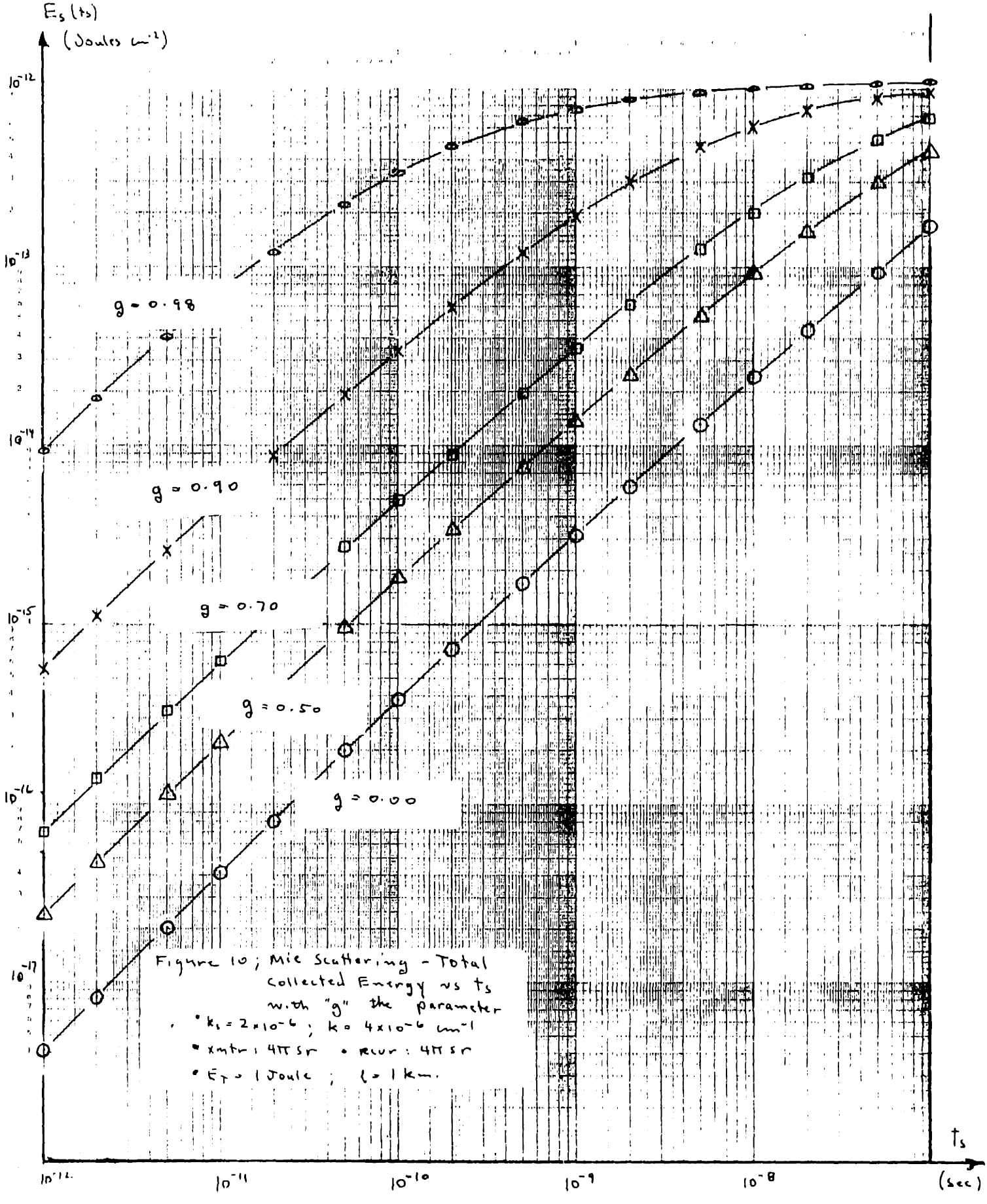

Figure 10; Mie Scattering - Total Collected Energy vs t_s with "g" the parameter

- $k_s = 2 \times 10^{-6}$; $k_o = 4 \times 10^{-6}$ cm^{-1}
- xmtr : 4π sr
- rcvr : 4π sr
- E_T = 1 Joule ; ℓ = 1 km.

THE FOLLOWING PAGES ARE PARTIALLY ILLEGIBLE

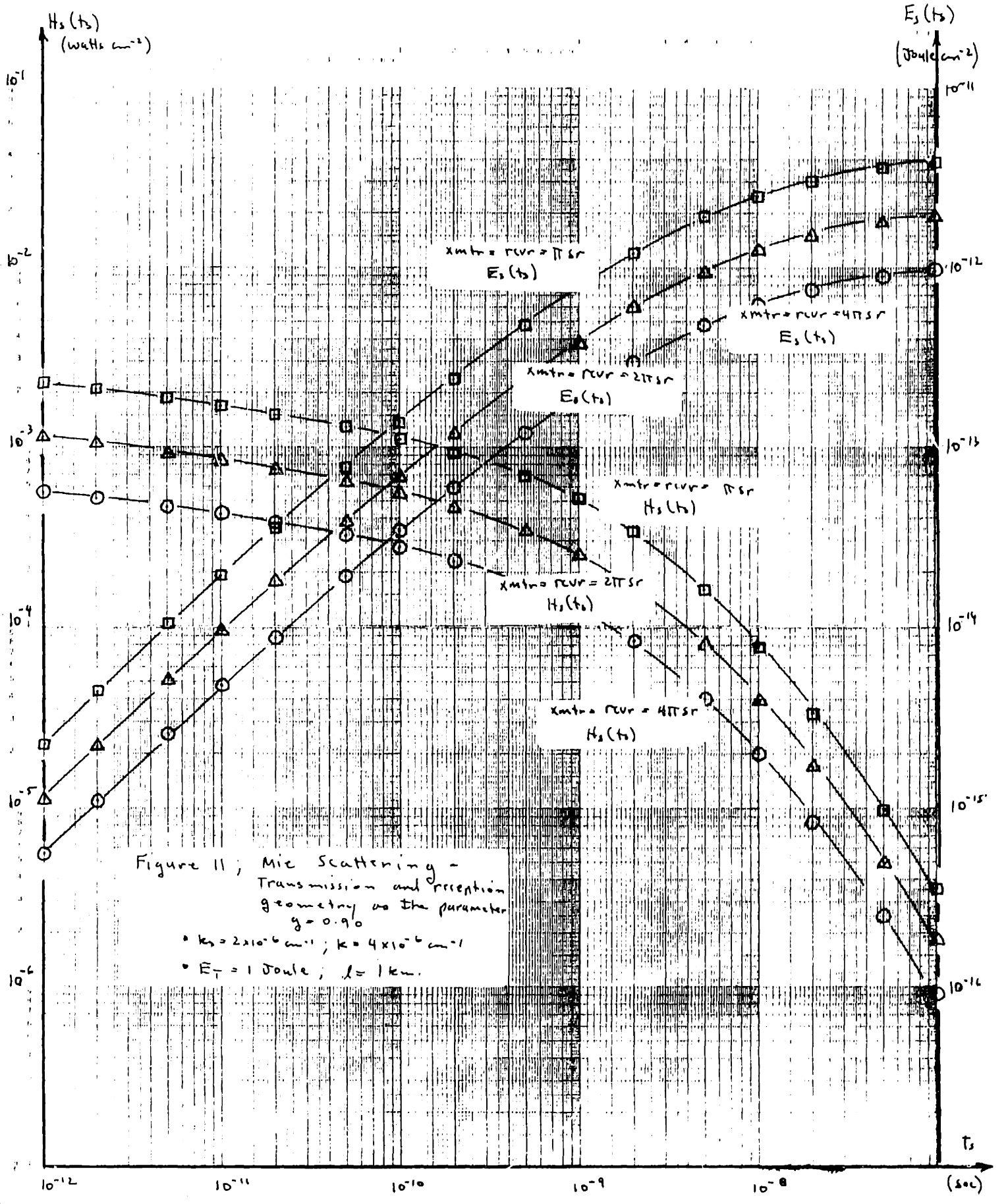

Figure 11; Mie Scattering - Transmission and reception geometry as the parameter
$g = 0.9$
- $k_s = 2 \times 10^{-6}$ cm^{-1}; $k = 4 \times 10^{-6}$ cm^{-1}
- $E_T = 1$ Joule; $l = 1$ km.

THE FOLLOWING PAGES ARE PARTIALLY ILLEGIBLE

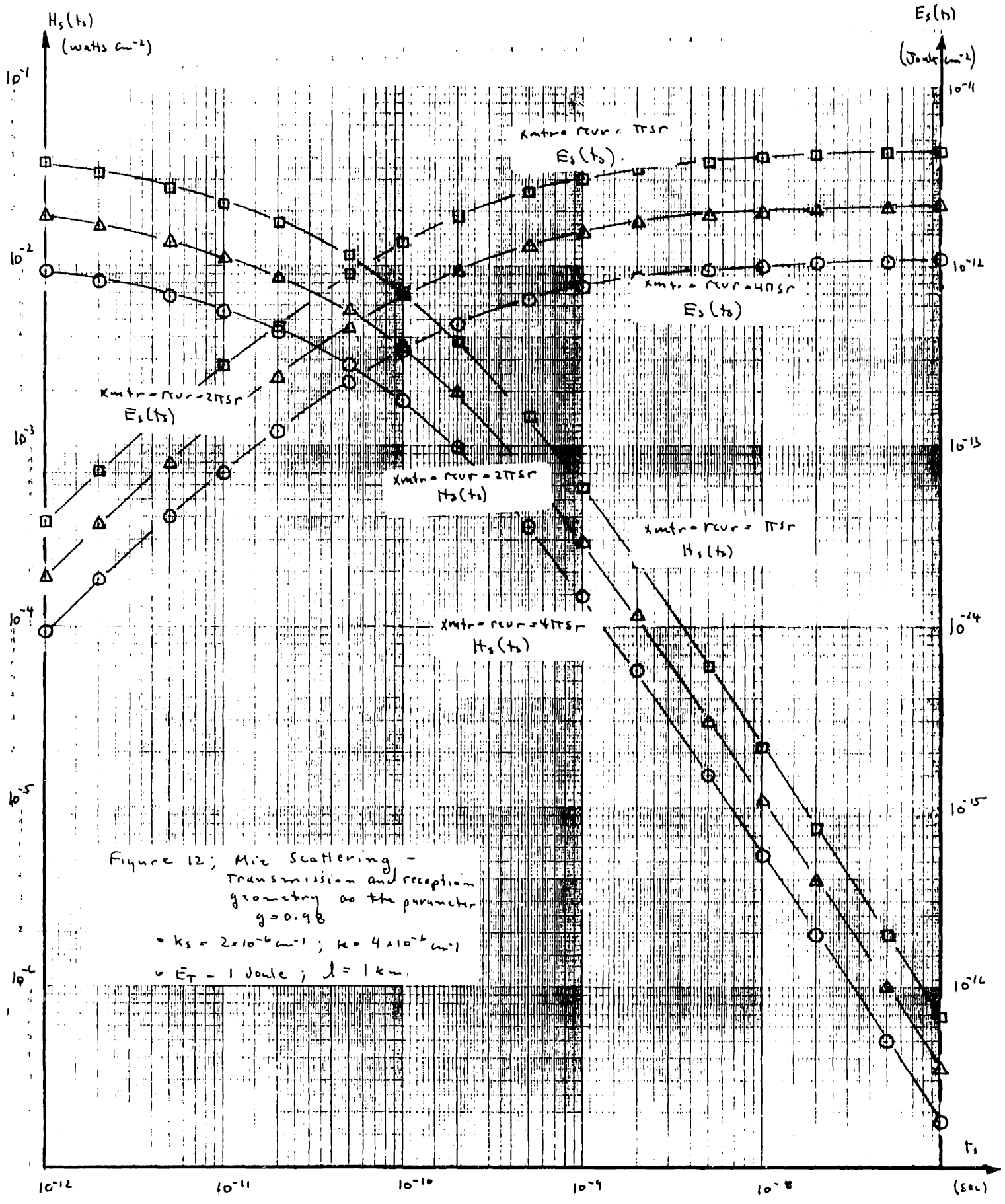

Figure 12; Mie Scattering - Transmission and reception geometry as the parameter $g = 0.98$

- $k_s = 2 \times 10^{-6}$ m^{-1} ; $k = 4 \times 10^{-6}$ m^{-1}
- $E_T = 1$ Joule ; $\ell = 1$ km.

THE FOLLOWING PAGES ARE PARTIALLY ILLEGIBLE

(f) Rayleigh and Mie Scatter Model: In reality, the scatter radiation field at the receiver is the sum of interactions with Rayleigh particles (gaseous molecules) and Mie particles (aerosols and precipatiting matter). This model determines the total irradiance and collected energy based on contributions from both Rayleigh and Mie Scattering. Figures 13 and 14 show the individual contributor and the totals for two different "g" values.

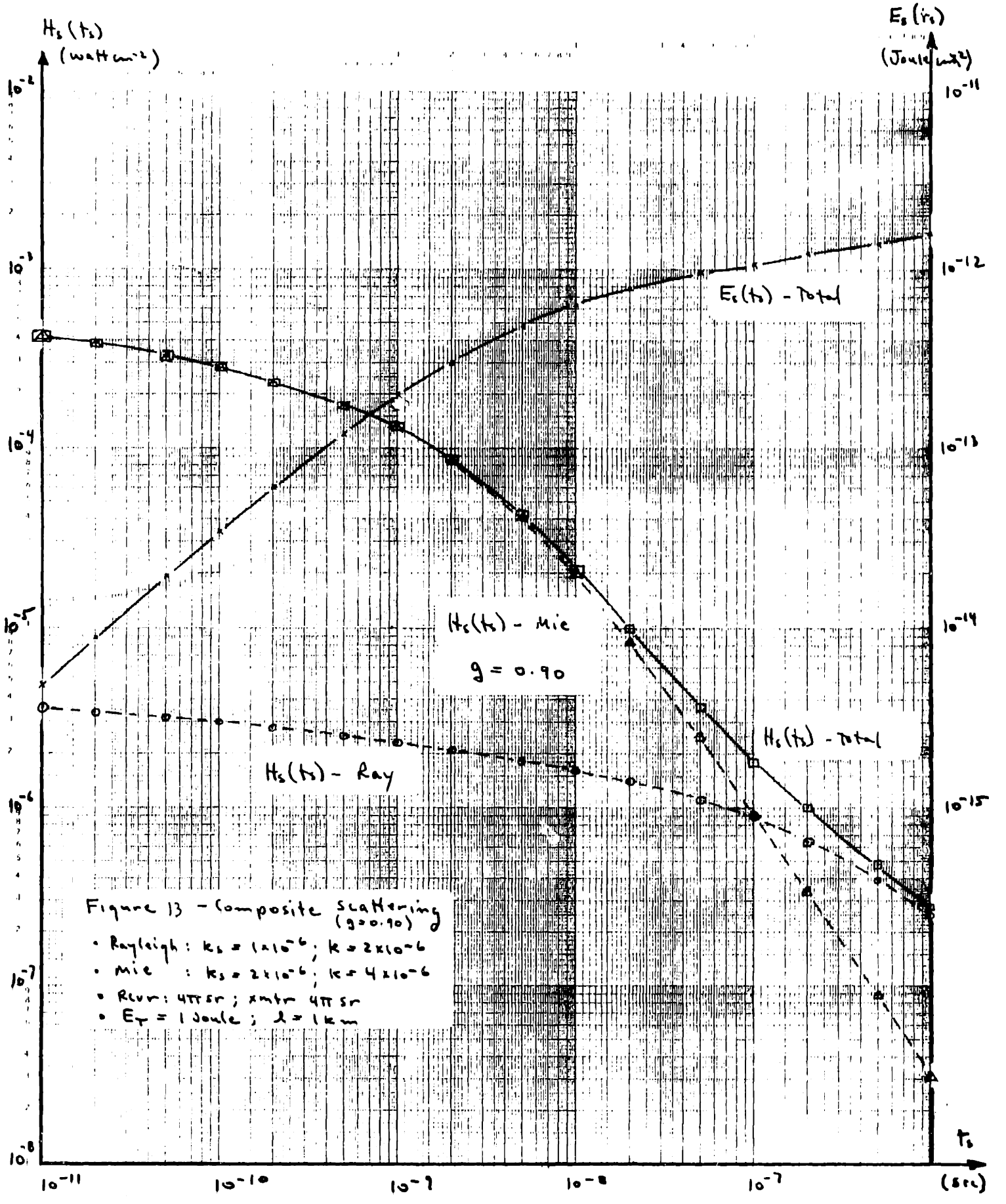

Figure 13 - Composite Scattering (g=0.90)

- Rayleigh : $k_s = 1 \times 10^{-6}$; $k = 2 \times 10^{-6}$
- Mie : $k_s = 2 \times 10^{-6}$; $k = 4 \times 10^{-6}$
- Rcvr: 4π sr ; xmtr 4π sr
- E_T = 1 Joule ; ℓ = 1 km

THE FOLLOWING PAGES ARE PARTIALLY ILLEGIBLE

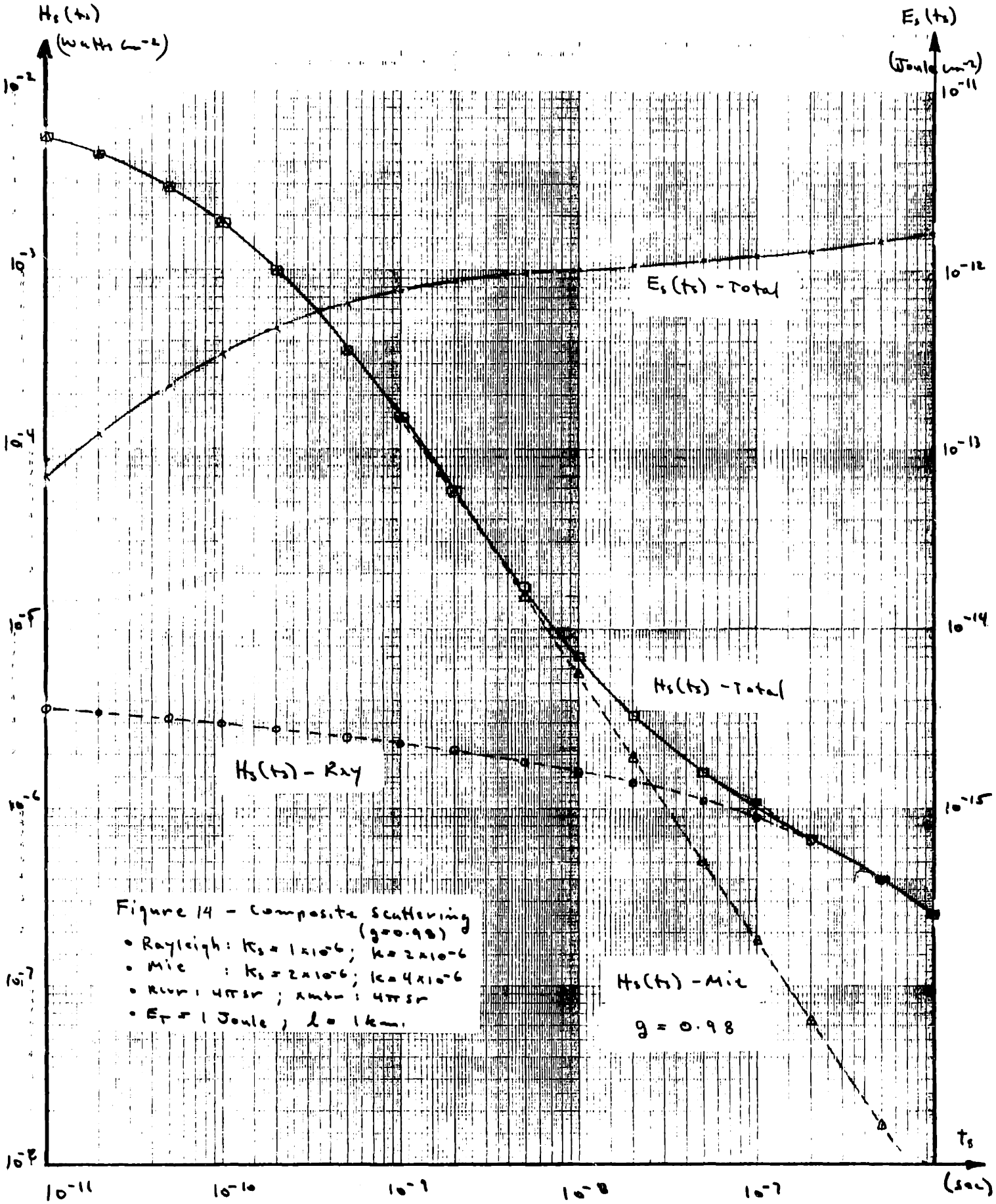

Figure 14 - Composite Scattering (g=0.98)

- Rayleigh: $K_s = 1 \times 10^{-6}$; $k = 2 \times 10^{-6}$
- Mie : $K_s = 2 \times 10^{-6}$; $k = 4 \times 10^{-6}$
- Ray : 4π sr ; Amb : 4π sr
- $E_T = 1$ Joule ; $l = 1$ km.

THE FOLLOWING PAGES ARE PARTIALLY ILLEGIBLE

4. PROPAGATION IN THE MIDDLE ULTRAVIOLET

In the middle ultraviolet, the atmosphere represents a highly absorbing and scattering medium. Absorption is primary due to ozone and oxygen and it is ultimately absorption by oxygen that renders the atmosphere opaque below 2000Å. Propagation thru the model atmospheres defined in Sections 2 and 3 is now considered. The interaction coefficients are listed in Section 3, Table 7. The distance from the transmitter to the receiver will be 0.25 km.

a) Extinction:

The amount of primary energy reaching the receiver from an isotropic transmitter is:

$$E_p = \frac{E_T}{4\pi} \quad \frac{e^{-k\ (0.25\ km)}}{(0.25\ km)^2} \quad \frac{Joules}{cm^2}$$

Values for E_p based on the extinction coefficients for the model atmospheres are listed in Table 1 for the wavelength and visual ranges of interest.

The attenuation (extinction) coefficients for the atmosphere in the middle ultraviolet were experimentally determined by Baum and Dunkelman[5] for a variety of conditions. Figure 15 represents a cross-section of the results obtained. The extinction coefficients developed in Section 3 from consideration of the

Wavelength λ (Å)	Visual Range (km)	Extinction Coefficient k (km^{-1})	Single Scatter Albedo $\overline{\omega}$	Transmission $\tau = e^{-k(0.25\ km)}$	Primary Energy E_p (Joules/cm^2)
2000	23	8.6×10^{-5}	0.15	0.12	1.5×10^{-11}
	5	1.0×10^{-4}	0.26	0.08	1.1×10^{-11}
2500	23	1.5×10^{-5}	0.43	0.69	8.8×10^{-11}
	5	2.8×10^{-5}	0.64	0.50	6.3×10^{-11}
3000	23	4.7×10^{-6}	0.92	0.89	1.1×10^{-10}
	5	1.7×10^{-5}	0.94	0.65	8.3×10^{-11}

TABLE 1: Extinction Coefficients, Transmission and Primary Energy

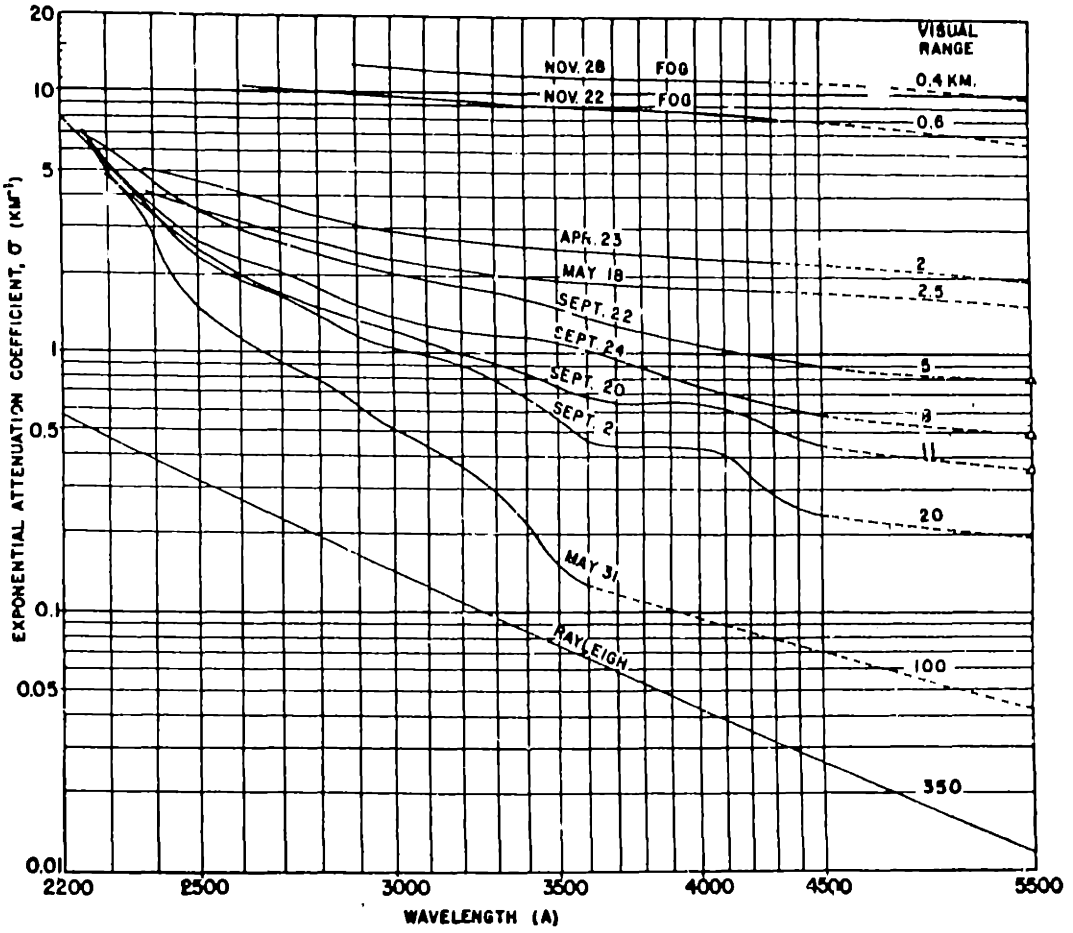

FIG. 7. Typical attenuation curves illustrating the full range of atmospheric conditions encountered at Pasadena in 1949. Triangles at 5500 A are based on visibility readings obtained with the Loofah haze-meter. Visual ranges for the other six nights are based on the dashed extrapolations of the attenuation curves. The theoretical Rayleigh curve for Pasadena is included for comparison.

FROM: W.A. Baum and L. Dunkelman, "Horizontal Anenuation of Ultraviolet Light by the Lower Atmosphere," Journal of The Optical Society of America; Vol. 45, Number 3, March 1955.

FIGURE 15: Measured Values for Atmospheric Attenuation Coefficients in the Middle Ultraviolet

basic properties of the atmospheric constituents agree as well as can be expected with those of Baum and Dunkelman.

b) Single Scatter:

The interaction coefficients defined in Section 3 (table 7) were utilized in conjunction with the composite scatter model to determine irradiance and collected energy vs t_s for several cases. The results are plotted in Figures 16 and 17.

Comparison of the collected energy characteristics (see figures 16 and 17 at λ = 2500 Å and 3000 Å for 5 Km and 23 Km visual ranges shows that they are almost identical even though both the absorption and scattering coefficients increase as decreases and the single scatter albedo goes from greater than 0.9 to approximately 0.5.

If the changes in primary energy as a function of visual range are compared with the corresponding changes in primary plus scattered energy, one observes a dramatic reduction. The comparative values are presented in table 2.

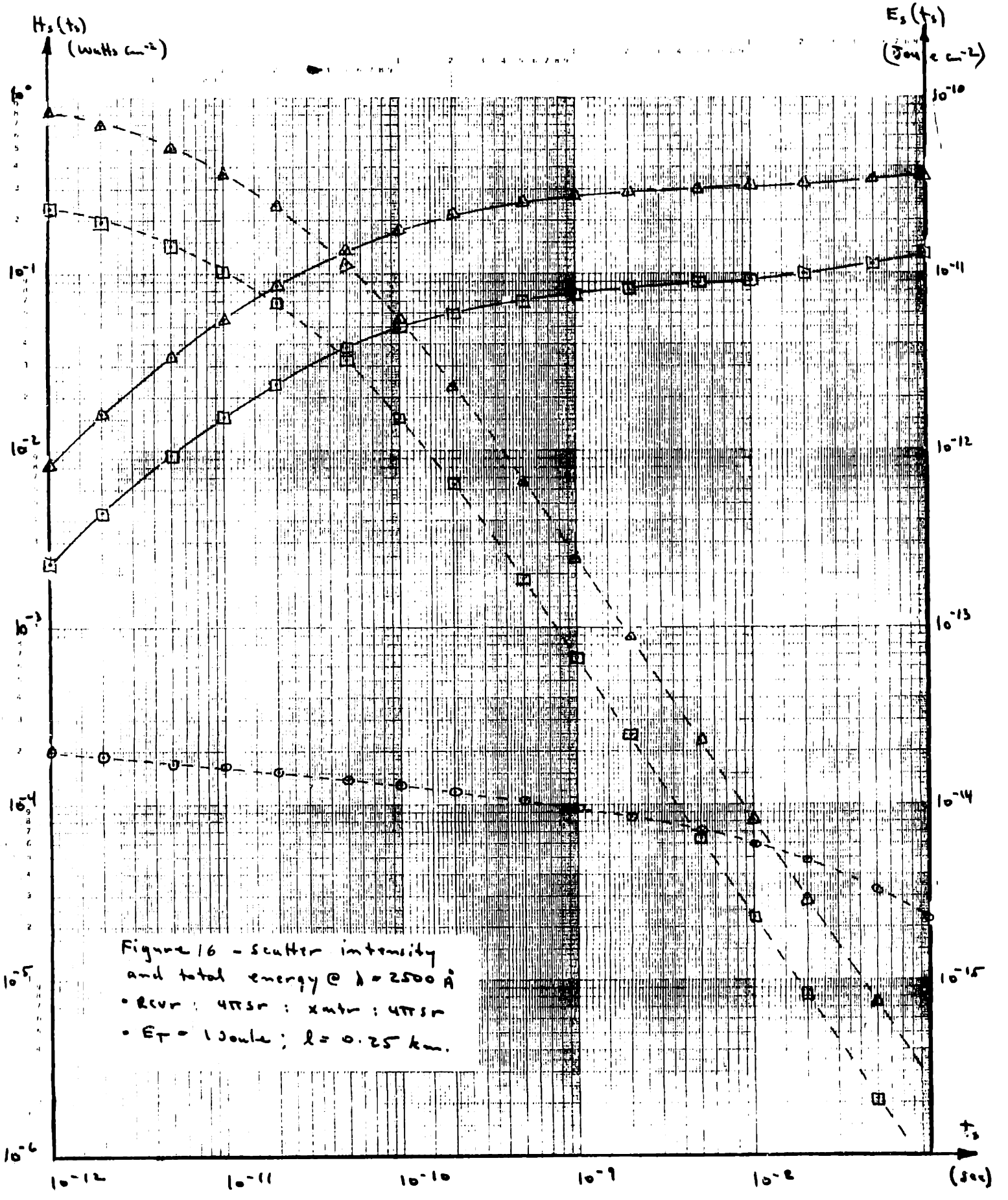

Figure 16 - Scatter intensity and total energy @ $\lambda = 2500$ Å
- Rcvr : 4π sr : Xmtr : 4π sr
- E_T = 1 Joule ; ℓ = 0.25 km.

THE FOLLOWING PAGES ARE PARTIALLY ILLEGIBLE

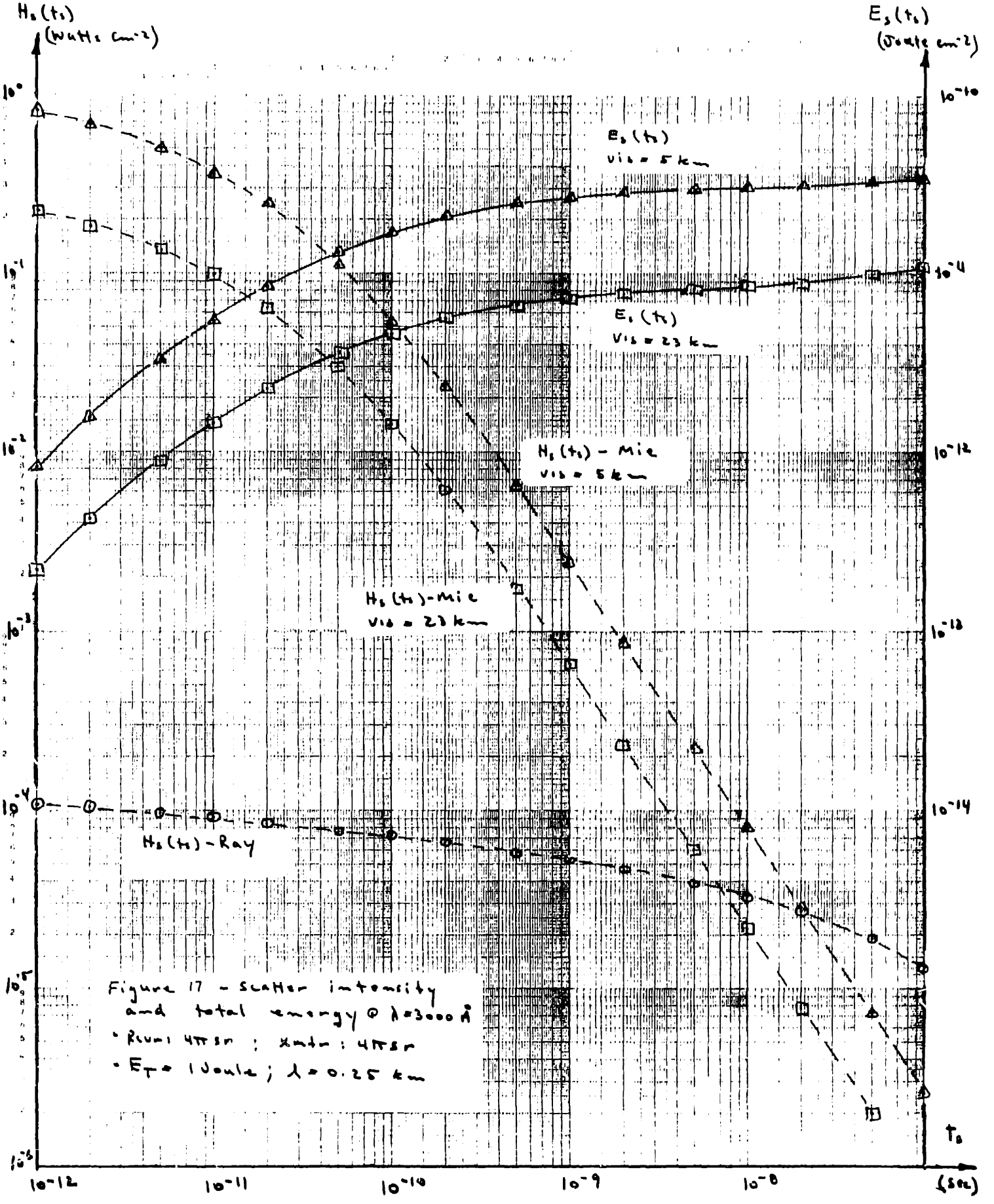

Figure 17 - scatter intensity and total energy @ λ = 3000 Å
- Runs 4π sr ; xmtr : 4π sr
- E_T = 1 Joule ; λ = 0.25 km

THE FOLLOWING PAGES ARE PARTIALLY ILLEGIBLE

Wavelength λ (Å°)	Visual Range (km)	total Scattered energy after 1 ns (Joule cm^{-2})	Primary energy (Joule cm^{-2})	Total energy = primary + scattered (Joule cm^{-2})		$\frac{Pri(23) - Pri(5)}{Pri(23) + Pri(5)} \times 100\%$ % change	$\frac{Tot(23) - Tot(5)}{Tot(23) + Tot(5)} \times 100\%$ % change
2500	5 km	2.75×10^{-11}	6.3×10^{-11}	9.05×10^{-11}		17 %	2.8 %
2500	23 km	0.78×10^{-11}	8.8×10^{-11}	9.58×10^{-11}			
3000	5 km	2.62×10^{-11}	8.3×10^{-11}	1.09×10^{-10}		14 %	3.6 %
3000	23 km.	0.72×10^{-11}	1.1×10^{-10}	1.17×10^{-10}			

TABLE 2: Primary vs. Total Scattered Energy After 1ns

References

1. V.E. Zuev, M.V. Kabanov, and B.A. Savelev, "Propagation of Laser Beams in Scattering Media," Applied Optics, January 1969, Vol. 8, No. 1

2. H.S. Steward and J.A. Curcio, "The Influence of Field-of-View on Measurements of Atmospheric Transmission," Journal of the Optical Society of America; Vol. 42, Number 11, November 1952.

3. R.O. Gumprecht and C.M. Sliepcevich, J. Chem. Phys., 57: 90-95 1953.

4. S. Chandrasekhar, Radiative Transfer, Dover, 1960.

5. W.A. Baum and L. Dunkelman, "Horizontal Anenuation of Ultraviolet Light by the Lower Atmosphere," Journal of The Optical Society of America; Vol. 45, Number 3, March 1955.

SECTION 5 - OPERATIONAL BACKGROUND

The ability of a receiver to detect small signals is generally determined by the noise environment in which the weak signal must be received. The noise environment is usually the result of several contributing sources both from within and external to the receiver. The predominance of one over the other is a function of many variables among which are: wavelength, receiver field-of-view, detection scheme and operational environment (i.e. space, terrestial, etc). It is the contribution from sources external to the receiver that this section addresses.

From 3000Å to 30000Å, the major source of background noise (during daytime) is solar radiation which is scattered by the atmospheric constituents on reflected from the earth's surface. Figure 1 shows the intensity of skylight as a function of wavelength with air mass as the parameter. At 3000Å the intensity is approximately 1-13mw cm^{-2} μ^{-1}.

For wavelengths between 0.2μ and 0.3μ, solar radiation is virtually totally absorbed in the upper atmosphere by ozone and molecular oxygen. Goody[1] estimates that at 2553Å (peak of ozone absorption) the transmission for solar radiation is about 10^{-66}.

Since solar radiation is insignificant in the middle ultraviolet, what determines the radiation background and what are it's spectral characteristics? Energetic electrons produced in the terrestial atmosphere by solar uv radiation (and cosmic rays) are thought to be the basic cause of many spectral emissions[2]. It is also expected that chemical reactions which are undoubtedly strongly influenced by the amounts of industrial and urban activity, will also be a source of background radiation.

If one assumes a background limited system where spectral filtering has effectively reduced all solar contributions, then it will be important to identify the contributors and their spectral characteristics in order to select an optimum operating wavelength and system geometry (Transmitter cone angle and receiver field-of-view).

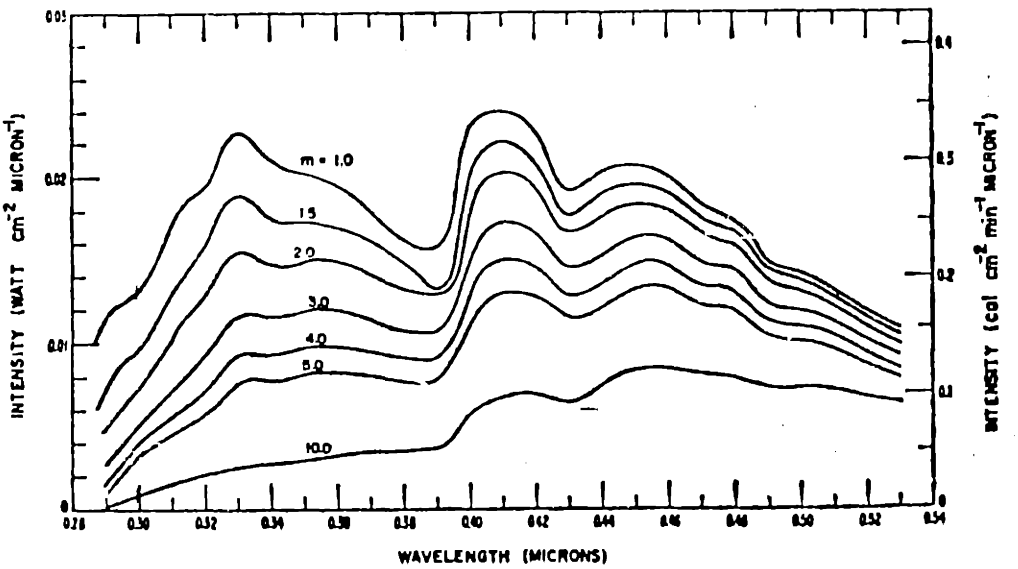

Fig. 6. Monochromatic intensity of skylight as a function of wavelength, for a sky in which Rayleigh scattering typically occurs, for solar-radiation slant paths corresponding to air mass 1.0, 1.5, 2.0, 3.0, 4.0, 5.0, and 10.0. Ground reflection with albedo = 0. [Data from Deirmendjian and Sekera (*20*)]

FROM: Gates, D.M., "Spectral Distribution of Solar Radiation at the Earth's Surface," Science, Vol. 151, Number 3710, February 4, 1966.

FIGURE 1: Intensity of Skylight vs Wavelength

References

1. R.M. Goody, Atmospheric Raidation I Theoretical Basis, Oxford, 1964, Page 209.

2. A.E.S. Green, et al; "Semi-Empirical Cross-Sections And The Airglow and Aurora," P. 523, In Atmospheric Emissions, McCormac and Omholt (1968).

SECTION 6 - CONCLUSIONS AND RECOMMENDATIONS

1. OPTICAL PROPERTIES OF THE ATMOSPHERE IN THE MIDDLE ULTRAVIOLET.

2. SINGLE SCATTER MODELS

3. PROPAGATION IN THE MIDDLE ULTRAVIOLET

---

1. OPTICAL PROPERTIES OF THE ATMOSPHERE IN THE MIDDLE ULTRAVIOLET

The interaction coefficients (absorption, scattering and extinction) and the single scatter phase function describe the interaction of radiation and the atmospheric constituents. In the middle ultraviolet, the coefficients and the asymmetry of the phase function are larger than those for the visible region and are highly dependent on wavelength. At 3000Å the extinction coefficient is predominally determined by scattering and single scatter albedos greater than 0.9 are experienced. As wavelength decreases, both the scattering and absorption coefficients increase; however, the predominance of scattering is reduced until the absorption and scattering coefficients are approximately equal at 2500Å. Below 2500Å absorption dominates and at 2000Å single scatter albedos of approximately 0.2 are experienced.

2. SINGLE SCATTER MODELS

The models developed for isotropic, Rayleigh and Mie type scattering and combinations of these, allow one to determine the instantaneous intensity at the receiver due to a transmitted

impulse. It may be thought of as the impulse response of the atmosphere for a particular atmospheric and system configuration. If the transmitted signal is a pulse, the received signal will be the convolution of the signal with the impulse response.

3. PROPAGATION IN THE MIDDLE ULTRAVIOLET

Propagation in the middle ultraviolet when compared to that in the visible, is not as sensitive to changes in meteorological conditions due to absorption and higher asymmetry of the phase function. This means that signal amplitude variations and time spreading will be reduced from that which would be experienced in the visible. Hence higher operating bandwidth should be possible in the middle ultraviolet. From the data contained on figures 19 and 20, one may conclude that high MHZ rates are possible with very small ($< 5\%$) amplitude variations for the range of atmospheric conditions considered. The lower wavelength boundary for useful propagation in the middle ultraviolet is established at $\lambda \simeq 2000\mathring{A}$ due to strong absorption by molecular oxygen.

APPENDIX 1

Prolate Spheroidal Coordinate System

The prolate spheroidal coordinate system is formed by rotating the two dimensional elliptic coordinate system, consisting of confocal ellipses, about the major axis of the ellipses. It is a right handed orthogonal curvilinear coordinate system. Details of this coordinate system are shown in Figures A1 and A2. Any point in space is determined by the values of the three coordinates ξ , η and ϕ where ξ is the radial coordinate, η the angular coordinate ($\eta = \cos \zeta$ where ζ is the angle between the major axis and the asymptote of a generating hyperbola) and ϕ the azimutal coordinate. Basic characteristics of this system are listed below:

1) Transformation - Prolate spheroidal to rectangular coordinates.

$$X = \frac{\ell}{2} \left[(1-\eta^2)(\xi^2-1)\right]^{1/2} \cos\phi$$

$$Y = \frac{\ell}{2} \left[(1-\eta^2)(\xi^2-1)\right]^{1/2} \sin\phi$$

$$Z = \frac{\ell}{2} \eta\xi$$

2) Range of Variables

$$1 \leq \xi \leq \infty$$

$$-1 \leq \eta \leq 1$$

$$0 \leq \phi \leq 2\pi$$

3) Scale Factors

$$h_\xi = \frac{\ell}{2} \left(\frac{\xi^2 - \eta^2}{\xi^2 - 1} \right)^{1/2}$$

$$h_\eta = \frac{\ell}{2} \left(\frac{\xi^2 - \eta^2}{1 - \eta^2} \right)^{1/2}$$

$$h_\phi = \frac{\ell}{2} \left[(1 - \eta^2)(\xi^2 - 1) \right]^{1/2}$$

4) Surface Area

$$dA = h_\eta \, d\eta \, h_\phi \, d\phi = \left(\frac{\ell}{2} \right)^2 \left[(\xi^2 - \eta^2)(\xi^2 - 1) \right]^{1/2} d\eta \, d\phi$$

$$A = \frac{\pi}{2} \ell^2 (\xi^2 - 1)^{1/2} \left[(\xi^2 - 1)^{1/2} + \xi^2 \sin^{-1} \left(\frac{1}{\xi} \right) \right]$$

5) Volume

$$dV = h_\xi \, d\xi \, h_\eta \, d\eta \, h_\phi \, d\phi = \left(\frac{\ell}{2} \right)^3 (\xi^2 - \eta^2) \, d\xi \, d\eta \, d\phi$$

$$V = \frac{\pi}{6} \ell^3 \xi (\xi^2 - 1)$$

6) Axes

major axis $= \ell \xi$

minor axis $= \ell (\xi^2 - 1)^{1/2}$

7) Interfocal Distance

interfocal distance $= \ell$

8) Eccentricity

$$e = \frac{1}{\xi}$$

FROM: C. Flammer, Spheroidal Wave Functions, Stanford University Press, 1957, P. 7, Fig. 1.

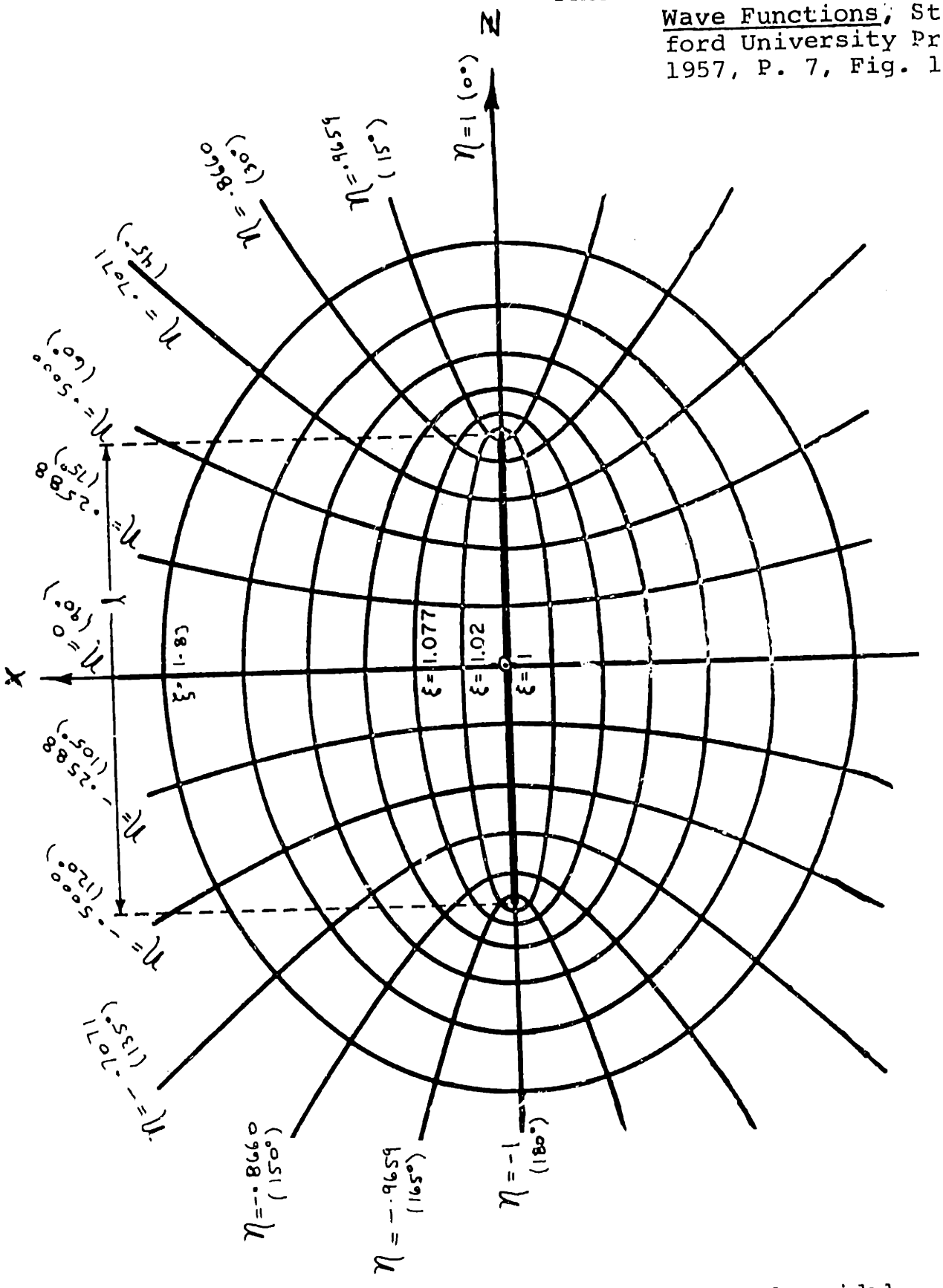

FIGURE A1: Cross-Section of Prolate Spheroidal Coordinate System

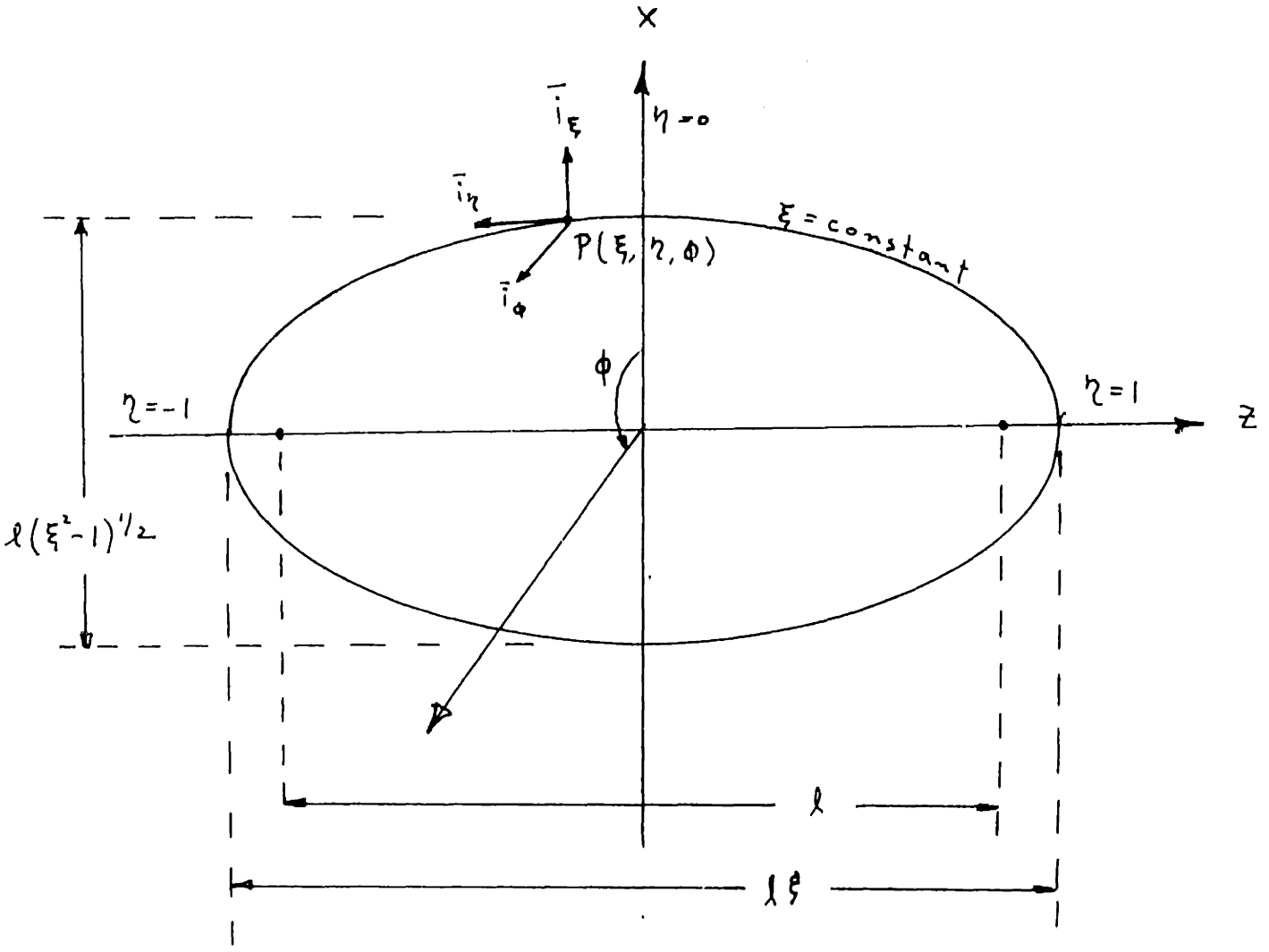

FIGURE A2: Unit Vectors for Prolate Spheroidal Coordinate System

References

1. G. Arfken, Mathematical Methods for Physicists, Academic Press, 1966

2. C. Flammer, Spheroidal Wave Functions, Stanford University Press, 1957.

3. NRL, Washington D.C., "Angular Spheroidal Wave Functions," Vol. I, Prolate m = 0.

APPENDIX 2

Evaluation of Integrals for Rayleigh Scattering

(1) $$\int \frac{1}{\xi^2 - \eta^2}\, d\eta = \frac{1}{2\xi} \ln\left(\frac{\xi+\eta}{\xi-\eta}\right)$$

(2) $$\int \frac{1}{\left(\xi^2-\eta^2\right)^2}\, d\eta = \frac{\eta}{2\xi^2(\xi^2-\eta^2)} + \frac{1}{2\xi^2}\int \frac{d\eta}{\xi^2-\eta^2}$$

$$= \frac{\eta}{2\xi^2(\xi^2-\eta^2)} + \frac{1}{4\xi^3} \ell n\left(\frac{\xi+\eta}{\xi-\eta}\right)$$

(3) $$\int \frac{1}{\left(\xi^2-\eta^2\right)^3}\, d\eta = \frac{1}{4\xi^2} \frac{\eta}{(\xi^2-\eta^2)^2} + \frac{3}{4\xi^2}\int \frac{d\eta}{(\xi^2-\eta^2)^2}$$

$$= \frac{1}{4\xi^2} \frac{\eta}{(\xi^2-\eta^2)^2} + \frac{3}{4\xi^2}\left[\frac{\eta}{2\xi^2(\xi^2-\eta^2)} + \frac{1}{4\xi^3} \ell n\left(\frac{+\eta}{\xi-\eta}\right)\right]$$

$$= \frac{\eta}{4\xi^2(\xi^2-\eta^2)^2} + \frac{3\eta}{8\xi^4(\xi^2-\eta^2)} + \frac{3}{16\xi^5} \ell n\left(\frac{\xi+\eta}{\xi-\eta}\right)$$

4) $$\int \frac{\eta^2}{(\xi^2-\eta^2)^2}\,d\eta = \frac{\eta}{2(\xi^2-\eta^2)} - \frac{1}{2}\int \frac{d\eta}{\xi^2-\eta^2}$$

$$= \frac{\eta}{2(\xi^2-\eta^2)} - \frac{1}{4\xi}\ln\left(\frac{\xi+\eta}{\xi-\eta}\right)$$

5) $$\int \frac{\eta^2}{(\xi^2-\eta^2)^3}\,d\eta = \frac{\eta}{4(\xi^2-\eta^2)^2} - \frac{1}{4}\int \frac{d\eta}{(\xi^2-\eta^2)^2}$$

$$= \frac{\eta}{4(\xi^2-\eta^2)^2} - \frac{1}{4}\left[\frac{\eta}{2\xi^2(\xi^2-\eta^2)} + \frac{1}{4\xi^3}\ln\left(\frac{\xi+\eta}{\xi-\eta}\right)\right]$$

$$= \frac{\eta}{4(\xi^2-\eta^2)^2} - \frac{\eta}{8\xi^2(\xi^2-\eta^2)} - \frac{1}{16\xi^3}\ln\left(\frac{\xi+\eta}{\xi-\eta}\right)$$

6) $$\int \frac{\eta^4}{(\xi^2-\eta^2)^3}\,d\eta = -\int \frac{\eta^2}{(\xi^2-\eta^2)^2}\,d\eta + \xi^2\int \frac{\eta^2}{(\xi^2-\eta^2)^3}\,d\eta$$

$$= -\frac{\eta}{2(\xi^2-\eta^2)} + \frac{1}{4\xi}\ln\left(\frac{\xi+\eta}{\xi-\eta}\right) + \frac{\xi^2\eta}{4(\xi^2-\eta^2)^2}$$

$$- \frac{\eta}{8(\xi^2-\eta^2)} - \frac{1}{16\xi}\ln\left(\frac{\xi+\eta}{\xi-\eta}\right)$$

$$= -\frac{5\eta}{8(\xi^2-\eta^2)} + \frac{3}{16\xi}\ln\left(\frac{\xi+\eta}{\xi-\eta}\right) + \frac{\xi^2\eta}{4(\xi^2-\eta^2)^2}$$